

IDENTIFICATION METHOD OF LONGITUDINAL COEFFICIENTS BASED ON THE NUMERICAL STUDY OF THE FLOW TOPOLOGY AROUND THE SACCON GEOMETRY

Baptiste Isnard¹, Geoffrey Tanguy¹, Dominique Farcy¹, Eric Garnier¹ & Jean-Marc Foucaut¹

¹Univ. Lille, CNRS, ONERA, Arts et Metiers Institute of Technology, Centrale Lille, UMR 9014 - LMFL - Laboratoire de Mécanique des Fluides de Lille - Kampé de Fériet, F-59000 Lille, France

Abstract

This paper focuses on improving the modelling of the unsteady and non-linear behaviour of the longitudinal aerodynamic coefficients of a generic UCAV configuration based on computational fluid dynamics (CFD). Conventionally, the changes in forces and moments during a trajectory of an aircraft are modelled with a first order Taylor series expansion of the aerodynamic coefficients. However, this kind of model does not allow to predict properly the non-linear behaviour observed at high incidence. Based on prescribed simulations of pitch forced oscillations at M=0.15, the application and implementation limitation of this classical linear reduced-order model (ROM) are highlighted. In order to improve the modelling accuracy of this ROM, the model parameters identification process is adapted to take into account the dynamics of the vortex flow during the motion. Thus, a multi-identification model is developed with parameters identified depending on the flow properties and the variations of flight parameters during forced oscillations. The multi-identification model proves to be able to reproduce more accurately the evolution of aerodynamic coefficients, during imposed trajectories, than either the classical linear model or the indicial method in the linear and non-linear flight domain.

Keywords: Reduced Order Models, Aerodynamic Coefficients, Delta Wing, CFD, Vortices

1. General Introduction

In flight dynamics, the correct modelling of the unsteady and non-linear nature of the behaviour in flight of an aircraft is still an active topic of research. Indeed, during the design phase, it is essential to be able to accurately assess the aircraft's stability and its performance. To this end, simulations of different trajectories must be carried out to study its flight behaviour. Different methods can be used. The first method, known as full-order model, consists in simulating full flight trajectories by performing unsteady CFD calculations [1, 2, 3]. However, setting up this type of study is very costly in terms of computation time, and requires a large number of simulations to characterize the general behaviour of the aircraft over the six degrees of freedom. The second approach, less expensive, is based on reduced-order models (ROMs). The ROMs are built to model the aircraft's aerodynamic torsor as a function of the flight conditions (Mach number M and Reynolds number R_e) and the flight parameters (angle of attack (AOA), angle of sideslip (AOS) and the rotation rates). In theory, they are used to quickly, easily and accurately predict the changes in the aerodynamic coefficients during a trajectory without having to perform a CFD simulation of a full flight trajectory [1, 2, 3, 4]. Nonetheless, these ROMs still require several CFD calculations to be implemented. However, these simulations are shorter and therefore less costly in total which justify their use. Among the various ROMs already developed, some need more or less simulations in order to be parameterized (such as the linear and non-linear indicial method [2, 5, 6]). The decision to use one ROM over another depends on the compromise between the accuracy and the computational cost that can be envisaged for a study. Whatever the precision and implementation cost of the ROM used, it allows to evaluate the controllable flight domain and carry out flight simulations at low cost compared with full-order models.

The accuracy of a ROMs is assessed by comparing its aerodynamic coefficients predictions over a trajectory with CFD results to assess the strengths and weaknesses of their modelling. The most common ROM is the linear Quasi-Steady model (QS model) [1, 3, 4, 5, 7, 8, 9], also known as stability derivative model. The linear model is made of dynamic derivatives, resulting from a first-order Taylor series expansion of the coefficients, determined from wind tunnel tests or numerical simulations of forced oscillations at fixed frequency and amplitude [1, 3, 4, 5]. The identification of the different dynamic derivatives can be carried out using the data of the oscillations in different ways, either by using the single point method [1, 3], the integral method [10, 11] or least squares method [1, 3, 5]. The results provided by these methods are similar because they all assume that the stability derivatives of the linear QS model are constant over a forced oscillation period. This assumption has no significant impact on the modelling of the coefficients in the linear flight domain. Indeed, at low incidence, the linear QS model has a good capacity to reproduce the changes in the aerodynamic coefficients during a trajectory [1, 5]. However, this assumption leads to identification and modeling problems in the stalled or near-stalled flight domain when non-linearities appear [4, 5, 12]. Discrepancies between the predictions of the linear QS model and the true behaviour of the aircraft have already been highlighted, particularly in the modeling of sudden variations in the aerodynamic coefficients [1, 12]. The main problem with this model is that it does not take into account the flow dynamics in its mathematical formulation and/or in the identification process of the stability derivatives. Furthermore, the linear QS model only depends on the current state of the aircraft and does not take into account the temporal evolution of the aircraft dynamics [4, 5, 13, 14]. Other ROMs, such as the unsteady linear model [5, 13, 15] or the indicial method [2, 5, 6], allow to take into account the influence of the aircraft's previous states and the dynamic variation of the rotation rate on the current behaviour. As a result, a slight improvement in performance has been observed compared with the linear QS model for modelling unsteady effects in the non-linear domain. However, in order to identify the parameters of the unsteady linear model or the non-linear indicial method, many more simulations and/or tests are required. This leads to higher computational costs for the implementation of the models [5]. Recently, NASA developed a multi-point method requiring the same number of tests or simulations as the linear QS model [12]. This method is designed to apply the single-point method for each data point of a forced oscillation loop. This new approach evaluates the stability derivatives of the model by making a distinction on the identification according to the sign of the rotation rate. This new model reproduces the changes in the aerodynamic coefficients much more accurately than the linear QS model. The disadvantage of this method is that each oscillation in the database is treated separately for the identification of the stability derivatives. Thus, the stability derivatives obtained overlap and are not continous over certain AOA ranges which makes the model unusable for the simulation of any flight manoeuvre.

The aim of this paper is to present a robust identification method for improving the application of the linear QS model in the non-linear domain. The method is inspired by the multi-point method proposed by the NASA [12]. It incorporates properties of vortex dynamics to identify the stability derivatives. Besides, all the oscillations loops are processed at the same time to identify the stability derivatives contrary to the multi-point method. Thus, it allows to identify a single value for each AOA and to obtain a continuous variation in the stability derivatives as a function of the AOA. The study is based on CFD calculations and focuses on the modeling of longitudinal coefficients.

The first two parts of this article present respectively the geometry studied and the coordinate systems used. The third part describes the numerical flow solver and the numerical methods and parameters of the simulations. The fourth part consists in validating the CFD code by comparing RANS calculations with wind tunnel tests. The last section is dedicated to the construction of a flight dynamics model. The linear QS model is presented and parameterised using URANS simulations of pitch forced oscillations. Once applied, the limitations of this model are highlighted. To improve this ROM, a new method of identification for the stability derivatives is developed based on the study of the flow dynamics. Finally, the multi-dientification method is compared with the initial linear QS model and with the results of the indicial method for the representation of aerodynamic coefficients during pitch forced oscillations.

2. Overview of the Geometry Studied and the Flight Dynamics Variables

2.1 The SACCON Geometry

The geometry as well as all the experimental data of the generic UCAV named SACCON (Stability And Control CONfiguration) were provided by the NATO RTO Task Group AVT-161 [16]. The SACCON was designed with a lambda wing planform with a sweep angle of 53°. The numerical study carried out here is based on the dimensions of the model manufactured by ONERA in 2010. The overall shape of the SACCON and its dimensions are presented in figure 1a and figure 1b. The root chord of the ONERA model is 0.689~m, its reference chord is equal to 0.3113~m and its half span is 0.5~m. The reference surface of the model is equal to $0.3253~m^2$. The moments are expressed at the moment rotation point (MRP) which is placed at 0.390~m from the nose of the aircraft i.e. x/l = 56.56%. This study is focused on the SACCON round leading edge (RLE) configuration for which the shape and the thickness of the leading edge is evolving [17]. The wing tip of this geometry is twisted by 5° around the leading edge to reduce the aerodynamic loads and shift the wing stall to higher angles of attack.

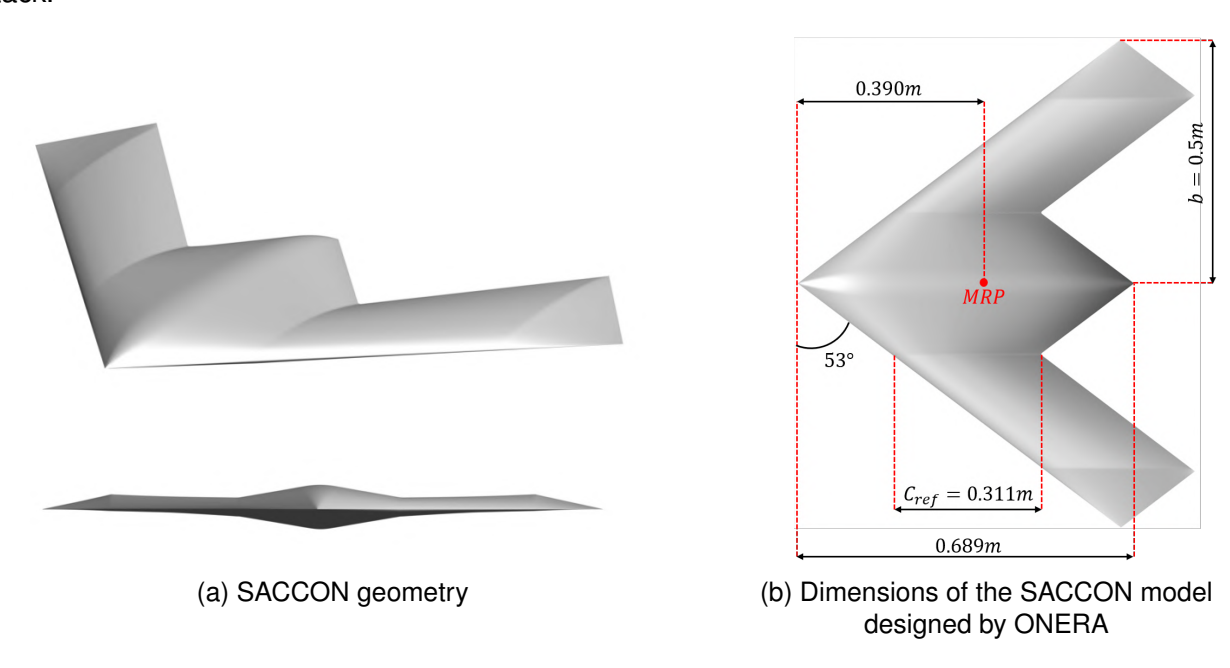


Figure 1 – Geometry of the SACCON (ONERA model)[5]

2.2 Coordinate System

For this study, a flight dynamics coordinate system is used (figure 2) to express forces and moments into the aircraft reference frame $\mathbf{R_p} = (\mathbf{O}, \mathbf{B_p} = (\mathbf{x_p}, \mathbf{y_p}, \mathbf{z_p}))$ or into the aerodynamic reference frame $\mathbf{R_a} = (\mathbf{O}, \mathbf{B_a} = (\mathbf{x_a}, \mathbf{y_a}, \mathbf{z_a}))$. The characteristic angles of the flight dynamics are then defined to switch from one to the other by a successive rotation of angles α and β corresponding respectively to the AOA and the AOS of the aircraft (figure 2). The origin of the coordinate system is arbitrarily chosen on the longitudinal axis of the aircraft and noted \mathbf{O} . This work focuses on longitudinal motions without any AOS which implies that only longitudinal aerodynamic coefficients are non-zero. Thus, only the drag, the lift and the pitch coefficients respectively noted C_D , C_L , C_m are studied. They are computed as follow:

$$C_D = -\frac{F_{x_a}}{\frac{1}{2}\rho V^2 S_{ref}} \qquad C_L = -\frac{F_{z_a}}{\frac{1}{2}\rho V^2 S_{ref}} \qquad C_m = \frac{M_{y_p}}{\frac{1}{2}\rho V^2 S_{ref} c_{ref}}$$
(1)

Where ρ is the density of the air, V is the speed of the aircraft relative to air at point \mathbf{O} , S_{ref} is the reference surface. For the rest of the paper, the reference chord will be noted c_{ref} and the half span of the aircraft noted b. For i=x, y or z, F_{i_a} is the force expressed in the aerodynamic coordinate system while M_{i_p} is the moment expressed in the aircraft coordinate system.

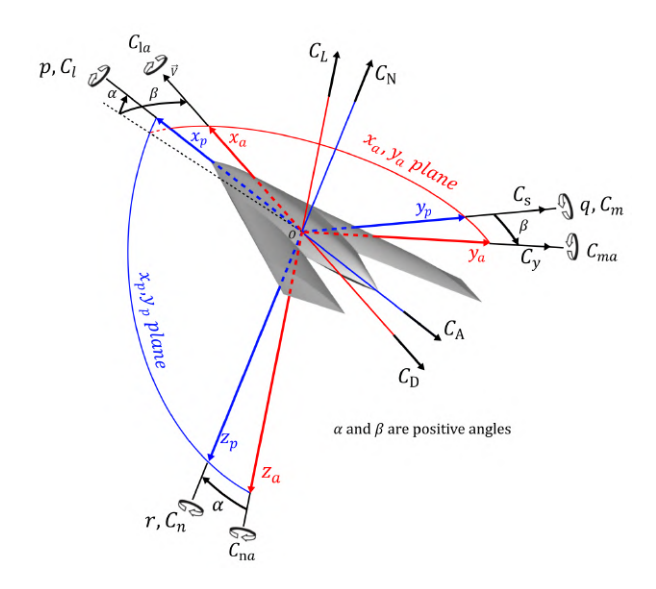


Figure 2 – Axes with force and moment orientation [5]

3. CFD Formulation

3.1 CFD Solver

The flow solver used for this study is the elsA code developed by the ONERA. The elsA code is a CFD code, based on a cell-centred "finite volume" approach, dedicated to the numerical simulation of internal and external flows for compressible and viscous fluids on two- and three-dimensional meshes. In particular, it allows parallel calculations for meshes with complex geometries in structured, unstructured or hybrid form. More details on the capabilities of this solver are described in Cambier et al. [18, 19]. In order to accelerate the solution of the discretised system, the elsA code uses an implicit method allowing a high Courant-Friedrichs-Lewy number (> 1). The diversity of models and simulation techniques present in this CFD code allows to adapt the simulations according to the problems and the different physical mechanisms encountered. In the context of our study, RANS and URANS calculations are performed.

3.2 Motion Simulation

The elsA code can simulate both free and specified six-degree-of-freedom (6-DOF) motions using mesh displacement. For this kind of simulation, a rigid body motion is applied. In the case of an imposed motion (case of this study), the trajectory is specified from an input file. The latter contains the location, at each time step, of the center of gravity of the aircraft and its orientation given by the roll, the pitch and the yaw angles according to the Tait-Bryan convention. The rigid body motion translates and reorients the mesh according to that input file. In the present work, the whole mesh is moving while the boundary conditions are fixed. The details of the method are described in Isnard et al. [5]. Simulations are performed in the relative speed frame $V_{\rm rel} + V_{\infty}$ where the velocity of the upstream flow V_{∞} is supposed constant. This grid motion technique is used to compute pitch forced oscillations and reproduce wind tunnel movements with URANS simulations.

3.3 Computational Grid and Numerical Parameters

To perform RANS and URANS simulations, a multi-block structured mesh is used (figure 3). The SACCON geometry is placed at the centre of a cylindrical domain with a radius and a height respectively equal to 20 and 40 times the size of the aircraft to minimize edge effects. The MRP (moment rotation point) of the SACCON is chosen as the origin of the frame. The total mesh size is about 25.5 million cells and results from a convergence study [20] in order to obtain the best agreement between numerical and experimental aerodynamic coefficients for a reasonable and acceptable restitution time. A particular attention has been paid to the resolution of the mesh at the leading edge, at the trailing edge and at the boundary layer in order to correctly capture the origin of the vortices (figure 3a). All CFD simulations are performed using the Spalart-Allmaras turbulence model [21] with

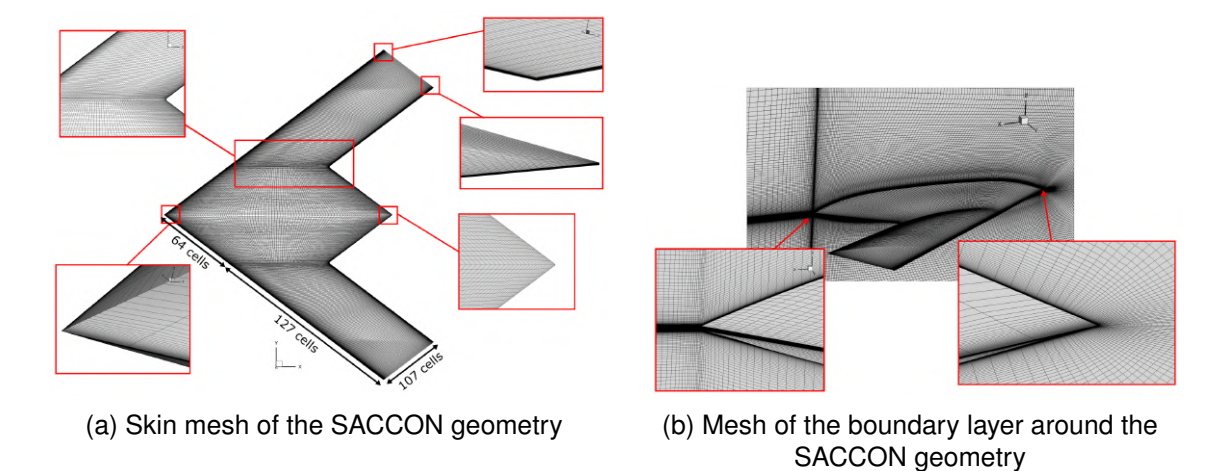


Figure 3 – Mesh used for simulations around the SACCON geometry [5]

the Jameson scheme (k_2 =0, k_4 = 0.016 to minimize the numerical dissipation) [22]. The elsA code solves the turbulence equations in a decentred way. So, the Harten parameter is set to a small value (0.01) to obtain a good accuracy [23]. An additional Martinelli correction (0.3) has also been added to improve the performance of the scheme and to avoid oscillation of the residuals. All calculations are performed in fully turbulent mode. Finally, low-Mach preconditioning [24, 25] is not used for this study because it turned out to be less accurate in reproducing the experimental static coefficients. The flow conditions are presented in Table 1. The SACCON surface is considered as an adiabatic rigid wall with no slip condition. Both RANS and URANS computations are launched on 224 cores. For the RANS simulations, the equations are solved using a backward Euler scheme and a CFL of 25 is applied to ensure a satisfactory speed of convergence (15h for 50000 iterations). URANS simulations are initialized from a steady state solution and two hundred iterations are performed before the motion starts in order to let the unsteady solution settled. The time integration method used to carry out the URANS simulations is a Gear method [26]. It is an implicit second-order method from the family of backward differencing methods. The solution at time $t + \Delta t$ is obtained from process of 20 sub-interations to achieve convergence. In this study, the URANS simulations are performed with a time step of $\Delta t = 5 \times 10^{-5} s$ (4h30 for 1000 iterations).

Table 1 – SACCON simulation parameters

Parameters	Values	Parameters	Values
Mach number M	0.15	Reynolds R_e	1.12×10^6
AOA $lpha$	−5° to 28°	\parallel AOS β	0°
Upstream Pressure P	101325 Pa	Density ρ	$1.2252 \ kg/m^3$
Temperature T	288 K	Viscosity μ	$1.7345 \times 10^{-5} Pa.s$
Upstream Velocity V	$51.04 \ m/s$	Turbulent Viscosity μ_t	$1.7345 \times 10^{-6} \ Pa.s$

4. Validation of the CFD Solver

4.1 Longitudinal Static Aerodynamic Coefficients

The drag, lift and pitch coefficients obtained numerically are compared with the results of DLR [27, 28] and ONERA [29, 30] wind tunnel tests for AOA ranging from -5° to 30° (figure 4). The CFD simulations closely reproduce the trends of experimental forces and moments up to moderate AOA. The offsets observed on the slopes of the lift coefficient C_L and pitch coefficient C_m can be explained by the absence of a sting in the CFD simulations [31]. For AOA higher than $\alpha = 17^{\circ}$, the flow around the wing is completely detached (figure 5d) and the Spalart-Allmaras turbulence model is not sufficiently accurate to correctly compute the flow topology. Thus, the changes in the numerical longitudinal coefficients are not well in line with tests. Nonetheless, the non-linear behaviour of the aerodynamic coefficients in the wind tunnel results is well reproduced by the CFD. It appears at $\alpha = 18^{\circ}$ and it is

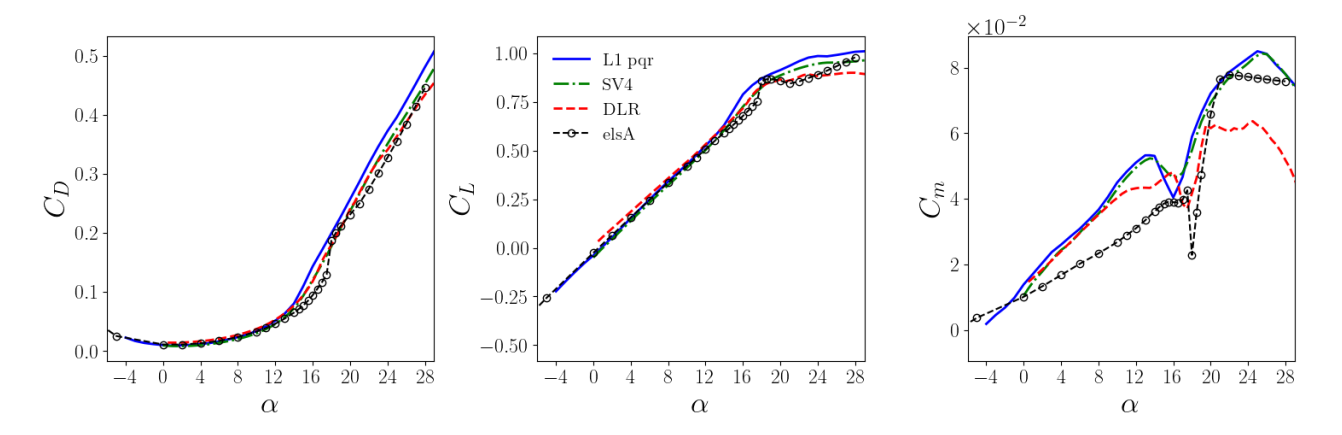


Figure 4 – Comparison between numerical (present work with elsA solveur at M=0.15 and $R_e=1.12\times 10^6$) and experimental static coefficients from ONERA (2011 tests in L1 [29] and SV4 [30] wind tunnels at M=0.103 and $R_e=0.75\times 10^6$) and DLR (TN2373 tests in DNW-NWB wind tunnel [27, 28] at M=0.149 and $R_e=1.6\times 10^6$) without AOS

particularly significant for the pitch coefficient C_m (figure 4). This comparison, between simulations and wind tunnel tests, shows that the elsA code is able to compute global forces and moments at low AOA, in relatively efficient way, and to reproduce the trends in the stall domain.

4.2 Characterisation of the Flow Topology

The CFD simulations allow to obtain an accurate restitution of the vortex dynamics trends, from the development of the vortices at around $\alpha=10^\circ$ (figure 5a) to their breakdown at around $\alpha=20^\circ$ (figure 5e). From $\alpha=10$ to 14° , the apex vortex and the tip vortex start to develop and their intensity increases (figure 5a). The location of the apex vortex is moved gradually toward the nose of the aircraft (figure 5b). From $\alpha=14$ to 16° , the apex vortex separates at the wing kink from the thickness vortex while the tip vortex intensifies but no longer rises towards the apex (figure 5b and c). Up to $\alpha=18^\circ$, the location of tip vortex is rapidly moving towards the nose of the aircraft which leads to a merger with the thickness vortex (figure 5d). This allows to explain the non-linearities observed in the aerodynamic coefficients (figure 4). Finally, the increase in the AOA leads to a progressive merging of

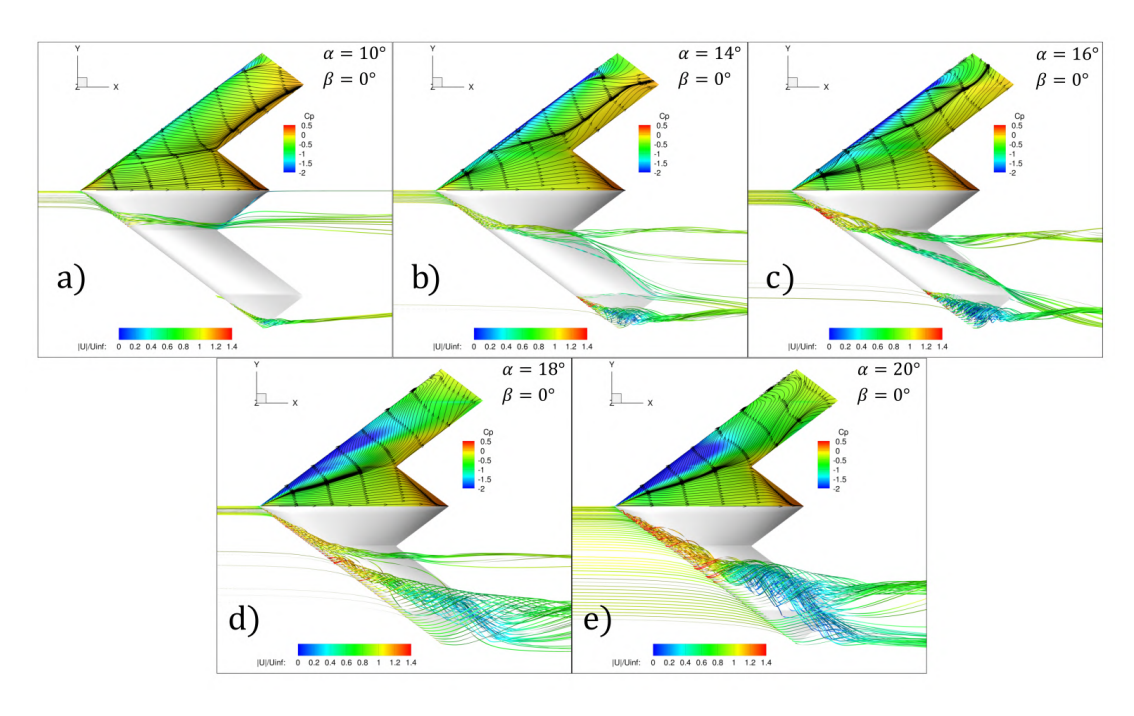


Figure 5 – Visualisation of the vortices on the upper surface of the SACCON obtained numerically for different AOA at M=0.15 and $R_e=1.12\times10^6$ without AOS [5]

the apex vortex and the tip vortex until the vortex breakdown (figure 5e). However, the experimental data obtained by PIV [17, 32] show that the numerical simulations fail to capture the development of these vortices for the correct AOA and their correct positions on the upper surface. Therefore, as for the aerodynamic coefficients, the CFD simulations properly reproduce the trends of the flow field with the variation of the AOA compared with experimental data.

5. Construction of a Flight Dynamics Model

In order to accurately model the trajectory and the aircraft's behaviour, the equations of flight dynamics have to be solved. Therefore, it is essential to know the value of the coefficients of the aerodynamic torsor at each instant as well as their variations as a function of the flight conditions (Mach number M and Reynolds number R_e) and the flight parameters (AOA, AOS and the rotation rates in roll p, pitch q and yaw r). To this end, reduced order models (ROMs) are used to model as accurately as possible the changes in the aerodynamic coefficients over time for a given trajectory as a function of the flight parameters.

5.1 The Linear Quasi-Steady Model (QS Model)

5.1.1 Presentation of the Model

The most common way of modelling the aerodynamic torsor is to express each coefficient as the sum of sub-coefficients depending on a subset of variables. These sub-coefficients, known as stability derivatives, are generally the results of a first order Taylor series expansion of the aerodynamic forces and moments [1, 4, 7, 8, 9, 6]. The present work focuses on longitudinal motion for a given speed. Longitudinal coefficients (C_D , C_L and C_m) are traditionnally written as follow:

$$C_i = C_{i_0} + C_{i_{\alpha}} \Delta \alpha + C_{i_{\alpha^*}} q^* + C_{i_{\dot{\alpha}^*}} \dot{\alpha}^* + C_{i_{\dot{\alpha}^*}} \dot{q}^*$$
 for $i = D, L, m$ (2)

Where $C_{i_0} = C_{i_0}(\alpha_0)$ represents the initial static aerodynamic coefficient and $\Delta \alpha = \alpha(t) - \alpha_0$ with $\alpha_0 = \alpha(t = 0)$. The above equation is expressed in terms of the following normalized quantities:

$$q^* = rac{q(t)c_{ref}}{V} \quad \dot{lpha}^* = rac{\dot{lpha}(t)c_{ref}}{V} \quad \dot{q}^* = rac{\dot{q}(t)c_{ref}^2}{V^2}$$

The impact of the deflection of control surfaces is not studied in this work and the coefficients related to their effects are not included in Eq.(2). In general, it is considered that the sub-coefficients vary according to the incidence α , the sideslip β and/or the Mach number M, in other words $C_{i_k} = C_{i_k}(\alpha, \beta, M)$ for $k = (\alpha, q^*, \dot{\alpha}^*, \dot{q}^*)$. In the present work, the effect of β and M on the coefficients are not studied which means that $C_{i_k} = C_{i_k}(\alpha)$. The identification of the stability derivatives is made possible by the study of pitch forced oscillations. The changes in the AOA during a pitch oscillation is written $\alpha(t) = \alpha_m + \alpha_k \sin(2\pi f t)$ with f, α_k and α_m respectively the frequency, the amplitude and the mean angle of the oscillation. For this imposed motion, a coupling appears between the AOA and the pitch rotation rate by the equation $\dot{\alpha}(t) = q(t)$. Thus, the drag coefficients C_D , the lift coefficient C_L and the pitch coefficient C_m can be written:

$$C_{i}(t) = C_{i_{0}} + \left(C_{i_{\alpha}} - \omega^{*2}C_{i_{q^{*}}}\right)\Delta\alpha + \left(C_{i_{q^{*}}} + C_{i_{\alpha^{*}}}\right)q^{*}$$

$$= C_{i_{0}} + C_{i_{\alpha+\hat{\alpha}^{*}}}\Delta\alpha + C_{i_{q^{*}+\hat{\alpha}^{*}}}q^{*} \qquad \text{for } i = D, L, m$$
(3)

Where the parameter $\omega^* = \frac{\omega c_{ref}}{V} = \frac{2\pi f c_{ref}}{V}$ corresponds to the normalized frequency of the pitch oscillation. $C_{i_{\alpha+q^*}}$ and $C_{i_{q^*+\alpha^*}}$ are respectively considered as the in-phase derivative and the out-phase derivative. Both of these parameters are determined for the mean angle of each oscillation using a least squares method over one period. To this end, the static coefficient C_{i_0} , obtained from RANS simulation, is subtracted from the aerodynamic coefficients obtained by CFD C_i^{osc} during a forced oscillation. Then, it is possible to write the following equation:

$$\begin{pmatrix} C_{i}^{osc}(t_{0}) - C_{i_{0}}(\alpha_{0}) \\ \dots \\ C_{i}^{osc}(t_{i}) - C_{i_{0}}(\alpha_{0}) \\ \dots \\ C_{i}^{osc}(t_{n}) - C_{i_{0}}(\alpha_{0}) \end{pmatrix} = \begin{pmatrix} \Delta\alpha(t_{0}) & q^{*}(t_{0}) \\ \dots & \dots \\ \Delta\alpha(t_{i}) & q^{*}(t_{i}) \\ \dots & \dots \\ \Delta\alpha(t_{n}) & q^{*}(t_{n}) \end{pmatrix} \begin{pmatrix} C_{i_{\alpha}}^{*} \\ C_{i_{q}}^{*} \end{pmatrix} \Leftrightarrow A = BC$$

$$(4)$$

where n is the number of time steps in an oscillation period and where the parameters of the matrix B, $\Delta \alpha$ and q^* , are known. Then, the stability derivatives of the matrix C are determined as follows:

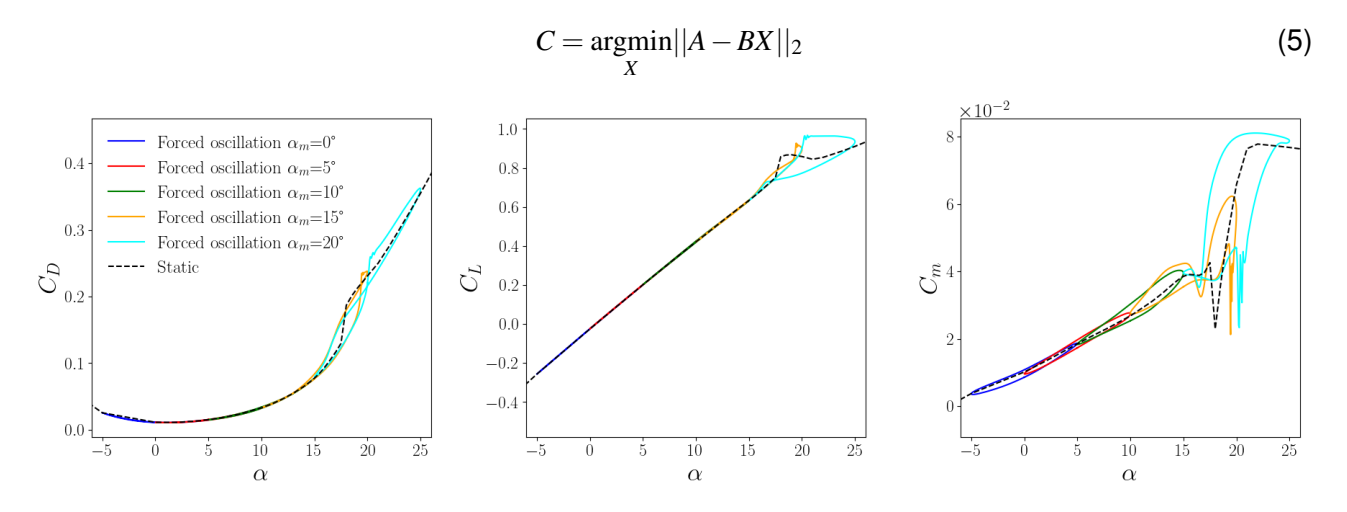


Figure 6 – Results of 1 H_Z pitch forced oscillations ($\omega^* = 0.03832$) of 5° amplitude centred in different AOA α_m at M = 0.15 and $R_e = 1.12 \ 10^6$ without AOS

5.1.2 Identification of Model Parameters from 1 Hz Forced Pitch Oscillations

Simulations of pitch forced oscillations were performed at M=0.15 using URANS calculations and the method of mesh displacement described in section 3.2. These simulations were carried out with the aim of reproducing ONERA's wind tunnel tests with a centre of rotation positioned at 0.438~m from the nose of the aircraft. The simulations were performed for an amplitude of 5°, a frequency of $1~Hz~(\omega^*=0.03832)$ and five different mean angles (0°, 5°, 10°, 15° and 20°). The changes in the drag, lift and pitch coefficients are shown in figure 6 and allows non-linear and unsteady effects to be observed. For low-AOA oscillations performed in the linear domain, i.e. centred on mean angles

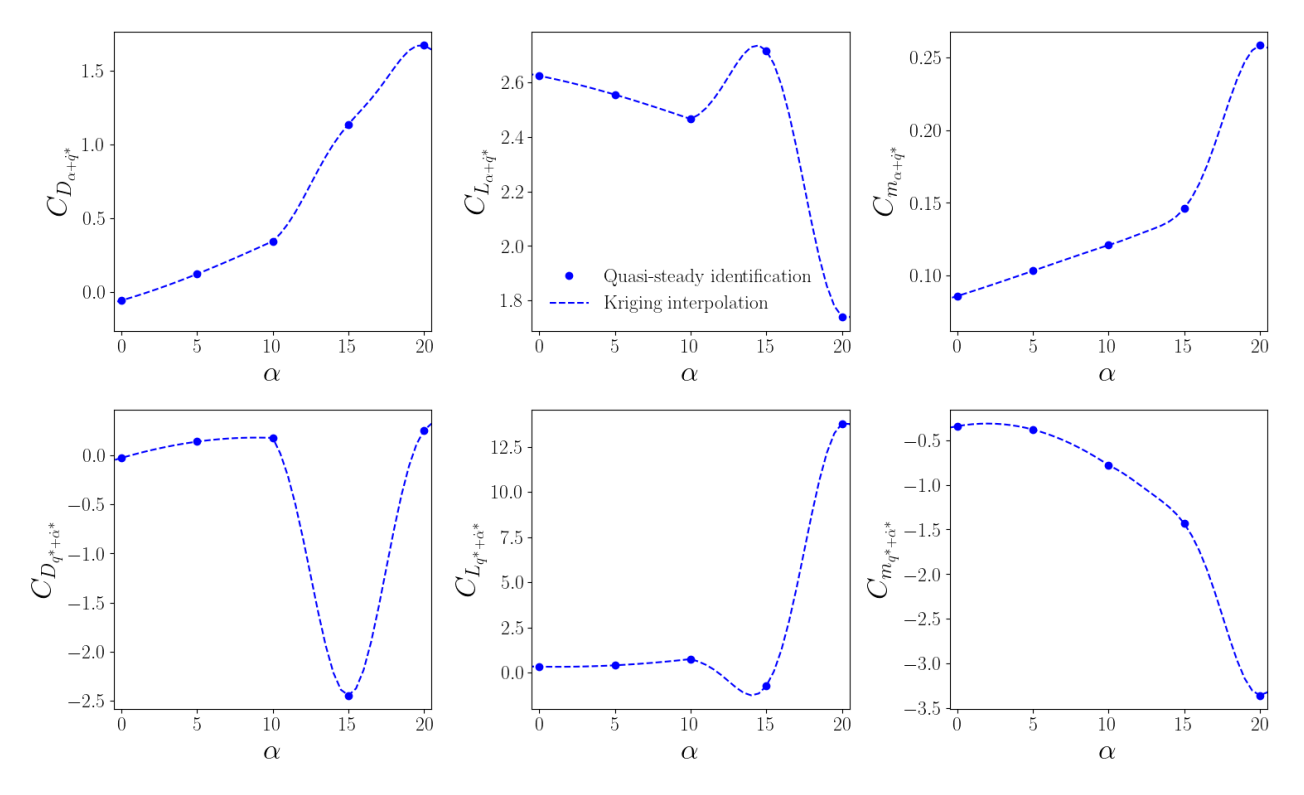
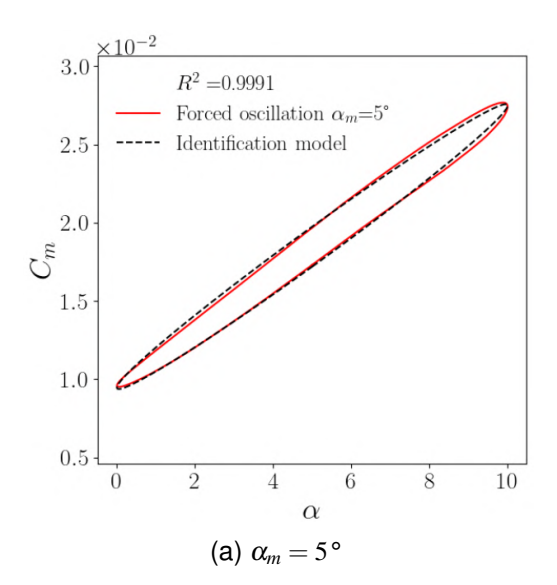


Figure 7 – In-phase derivative $C_{i_{\alpha+q^*}}$ and out-phase derivative $C_{i_{q^*+\alpha^*}}$ as a function of the AOA determined from 1 H_Z pitch forced oscillations ($\omega^* = 0.03832$) of 5° amplitude

between $\alpha_m = 0^{\circ}$ and $\alpha_m = 10^{\circ}$, only slight dynamics hysteresis phenomena are revealed (figure 6). The changes in the aerodynamic coefficients with the variation of the AOA no longer follows the static curve but forms an ellipse around it. A misalignment of the axis of the ellipse with the static curves is observed. This phenomenon is more significant on the pitch coefficient C_m (figure 6). For forced oscillations with higher mean angle ($\alpha_m = 15^{\circ}$ and $\alpha_m = 20^{\circ}$ light blue and orange curves in figure 6), the CFD predicts a strongly non-linear behaviour in addition to hysteresis phenomena. These non-linearities are similar to those observed in the static curves but shifted toward higher or lower AOA which may suggests that the dynamics of the aircraft cause a delay in the vortex dynamics. This phenomenon is very well observed with the drop on the pitch coefficient C_m (figure 6). Based on these simulations, the stability derivatives $C_{i_{\alpha+\dot{\alpha}^*}}$ and $C_{i_{\alpha^*+\dot{\alpha}^*}}$ are determined at the mean angle of the oscillations (0°, 5°, 10°, 15° and 20°) thanks to Eq.5 and shown in figure 7. These coefficients appears to be dependent on AOA as expected [4, 13, 14]. Kriging-type interpolation is performed to estimate these parameters at each AOA (figure 7) and to be able to apply the linear QS model (Eq.3). This kriging interpolation is based on the MultiFiCoKriging algorithm of the open source library OpenMDAO [33]. The optimal hyperparameters of the kriging model are estimated by a maximum likelihood optimization presented by Sacks et al. [34]. This optimisation problem is solved iteratively until the hyperparameters converge, using the L-BFGS-B (Limited-memory Broyden Fletcher Goldfarb Shanno Bound-constraint) gradient descent method introduced by Byrd et al.[35].

5.1.3 Limitation of the Model

The identification process of the in-phase derivative $C_{i_{\alpha+\hat{q}^*}}$ and the out-phase derivative $C_{i_{q^*+\alpha^*}}$ assumes that the value of both coefficients depends on the mean angle of the forced oscillation but remains constant over an oscillation loop. The validity of this approach is questionable. Performing the identification by considering the parameters constant over a period is not justified for all AOA and can lead to modeling inaccuracies. To illustrate our remarks, studies will be carried out on the pitch coefficient C_m , which exhibits the most pronounced hysteresis effects and non-linearities. This approximation gives satisfactory results in the linear flight domain, where the linear QS model parameters do not vary significantly (figure 8a). However, at high AOA, the behaviour of the aircraft becomes non-linear, due to the vortex-dominated flow on the upper surface of the wing. In this flight envelope, the assumption that the coefficients do not vary over an oscillation period are no longer valid (figure 8b). The identification process does not correctly capture the non-linear evolution of the pitch coefficient C_m . Thus, the stability derivatives of linear QS model cannot be correctly identified when non-linearities appear which means that the prediction of the aircraft's behaviour are incorrect in the non-linear domain. Moreover, the ROM formulation, given by Eq.(3), can only be used to model



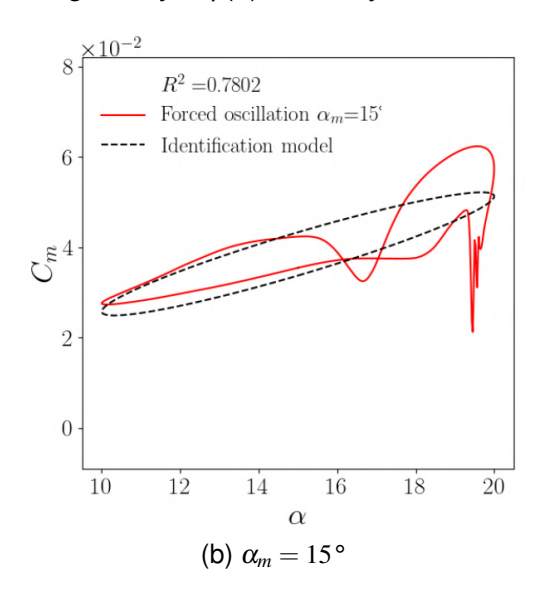


Figure 8 – Representation of the identification model applied to a 1 H_Z CFD pitch forced oscillation period ($\omega^* = 0.03832$) of 5° amplitude centered on different mean angles α_m

forced oscillations around a given AOA due to the parameter $\Delta\alpha$. Classically, to model other kind of trajectories, the dynamic damping coefficient $C_{i_{q^*}}$ in Eq.(2) is neglected and the static derivative $C_{i_{\alpha}}$ is merged with the static coefficient. Thus, the longitudianl aerodynamic coefficients are written as follow:

$$C_i = C_{i_0}(\alpha(t)) + C_{i_{\alpha^* + \dot{\alpha}^*}} q^*$$
 for $i = D, L, m$ (6)

Where $C_{i_0}(\alpha(t))$ represents the static coefficient evaluated in $\alpha(t)$. This new formulation results in a loss of information on the value of the dynamic damping coefficient $C_{i_{q^*}}$, which can be a handicap to model accurately the aircraft's behaviour.

5.1.4 Application of the Model

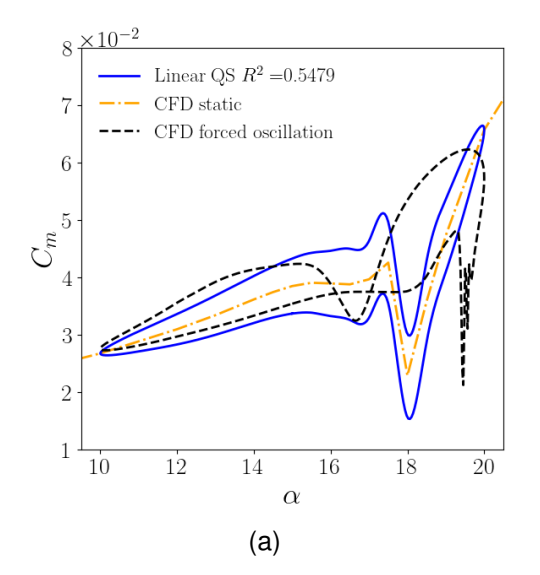
The ability of the models to reproduce the changes in aerodynamic coefficients during a flight trajectory is assessed by comparison with CFD data. The aerodynamic coefficients obtained during a CFD simulation are directly compared with those given by the ROM for a given set of trajectory parameters. The overall accuracy of the model is evaluated using the coefficient of determination R^2 :

$$R^{2} = 1 - \frac{\sum_{i=1}^{n} \left(C_{i}^{CFD} - C_{i}^{ROM} \right)^{2}}{\sum_{i=1}^{n} \left(C_{i}^{CFD} - mean(C_{i}^{CFD}) \right)^{2}}$$
(7)

The instantaneous modelling error is computed as a percentage with the following formulation [6]:

$$C_i \ ROM \ error = \left| \frac{C_i^{ROM} - C_i^{CFD}}{max(C_i^{CFD}) - min(C_i^{CFD})} \right| \times 100$$
 (8)

The linear QS model (Eq.6) is applied and compared with the CFD data of a 1 Hz pitch forced oscillation period ($\omega^*=0.03832$) of 5° amplitude centered on a mean angle of $\alpha_m=15$ ° (figure 9a). Overall, the model does not correctly represent the changes in the pitch coefficient or its trends. Indeed, the non-linearities observed in the CFD simulations are not reproduced by the ROM. As a result, the overall accuracy of the model is poor over the entire imposed trajectory. It is characterised by a low coefficient of determination $R^2=0.5479$. An instantaneous study of the error (Figure 9b) between the model prediction and the CFD calculation confirms the poor reproduction of the pitch coefficient changes by the ROM. The discrepancies are particularly large, up to 60% in the non-linear domain for AOAs greater than 15° (corresponding to t between 0 and t of t between 0 and 0.5 t of this ROM to reproduce forces and moments in the linear domain. Thus, the linear QS



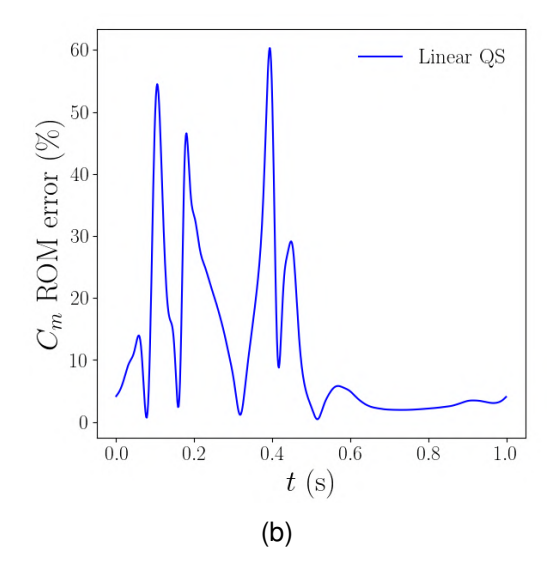


Figure 9 – Comparison between the changes in the pitch coefficient C_m obtained by CFD calculation and by the linear model QS a), and the associated instantaneous error b) during a 1~Hz pitch forced oscillation period ($\omega^* = 0.03832$) of 5° amplitude centered on a mean angle of $\alpha_m = 15$ °

model does not allow the representation of non-linearities, which limits its use when flow separations, interaction between vortices or vortex breakdown occurs. To improve this model, the identification process needs to be reviewed to take into consideration that the aircraft behaviour is dictated by the vortex flow on the upper surface of the wing. Indeed, the current identification process assumes that vortex dynamics is unaffected by motion which implies that variations in flow topology are not taken into account in the model.

5.2 Flow Topology During a Forced Oscillation

The aim of this section is to identify the correlation between the vortex dynamics and the changes in the aerodynamic coefficients during a forced oscillation. In this way, a method for identifying the stability derivatives of the linear QS model based on the flow topology could be established. In order to observe significant differences between the static and dynamic flow topology, the study of the vortex dynamics is carried out on a $3\,H_Z$ pitch forced oscillation period ($\omega^*=0.11497$) of $5\,^{\circ}$ amplitude centered on a mean angle of $\alpha_m=15\,^{\circ}$. The study focuses on the pitch coefficient C_m , which exhibits the most pronounced hysteresis effects and non-linearities. The C_p (figure 10) and the vortex flow (figure 11) obtained at four characteristic points of the oscillation are compared with the static case taken at the same AOA:

- a) during the decreasing AOA phase $q=q_{min}<0$ and $\dot{q}=0$ at $\alpha=15^{\circ}$
- b) at the end of the decreasing AOA phase q=0 and $\dot{q}>0$ at $\alpha=10^{\circ}$
- c) during the increasing AOA phase $q = q_{max} > 0$ and $\dot{q} = 0$ at $\alpha = 15$ °
- d) at the end of the increasing AOA phase q=0 and $\dot{q}<0$ at $\alpha=20^{\circ}$

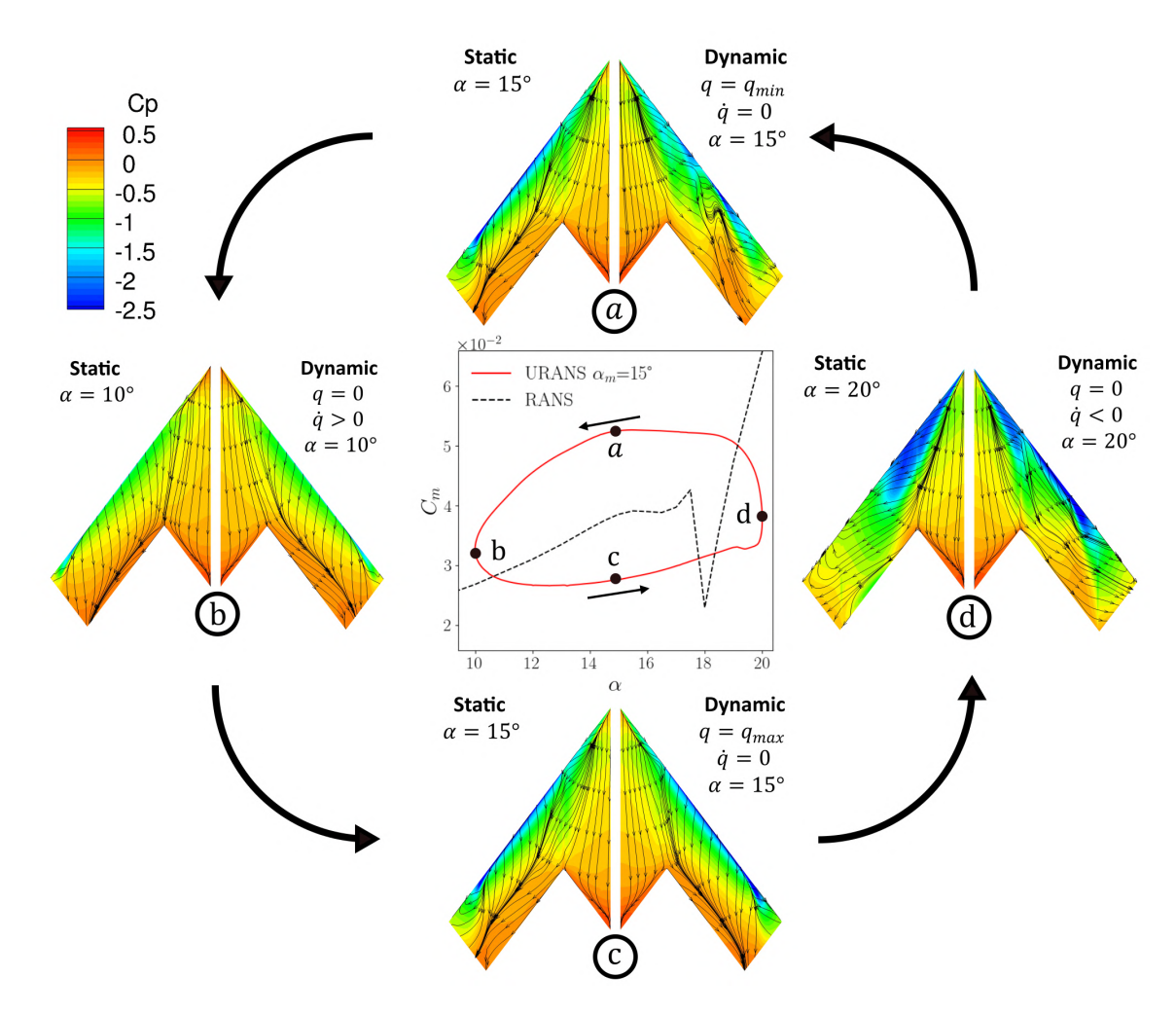


Figure 10 – Comparison of static and dynamic C_p at four instants of a 3 H_Z pitch forced oscillation period ($\omega^* = 0.11497$) of 5° amplitude centered on a mean angle of $\alpha_m = 15$ °

Comparison of dynamic and static C_p at the same AOA clearly shows differences in local pressure distribution (figure 10). These differences in the parietal pressure are therefore at the root of the dynamic effects observed on the aerodynamic coefficients and can be related to the difference between the flow topology (figure 11). Friction lines can also be used to visualize differences in flow separation zones (figure 10). Taking points b) and d), for which rotation rates are zero (q = 0), differences are observed compared with the static cases. At point b), the vortex flow is slightly developed (figure 11), which explains the small differences in the C_p (Figure 10) between the static and the dynamic case. However, some differences are observed in the position of the friction lines which indicate that the separation is more significant on the upper surface of the wing in the dynamic case (Figure 10). At point d), the vortex flow is fully established. Between the static and dynamic case, significant differences in the topology of the flow are observed on the number of vortices present on the upper surface of the wing, their position and their intensity (figure 11). This leads to the different low parietal pressure areas observed with the pressure coefficient C_p (figure 10). These differencies, between static and dynamic case, are linked to hysteresis effects caused by aircraft motion and the more developed the vortex flow, the more pronounced the effect. These phenomenon can be associated with the variation in rotation rate which is non-zero ($\dot{q} \neq 0$). In addition, the changes in the C_p (figure 10) and the flow topology (figure 11) during the increasing AOA phase ($b \rightarrow c \rightarrow d$) appears to be different from the decreasing phase $(d \to a \to b)$. Indeed, the pressure coefficient C_p , the friction lines and the flow topology of points a) and c) are completely different. However, these points are located exactly at the same AOA but at different phases of the oscillation. Points a and c are respectively from a phase of decreasing (q < 0) and increasing (q > 0) AOA. This suggests a difference in flow behaviour as the aircraft AOA increases or decreases. All these flow properties are not taken into account in the linear QS model, which limits its performance in modelling aerodynamic coefficients in the non-linear domain.

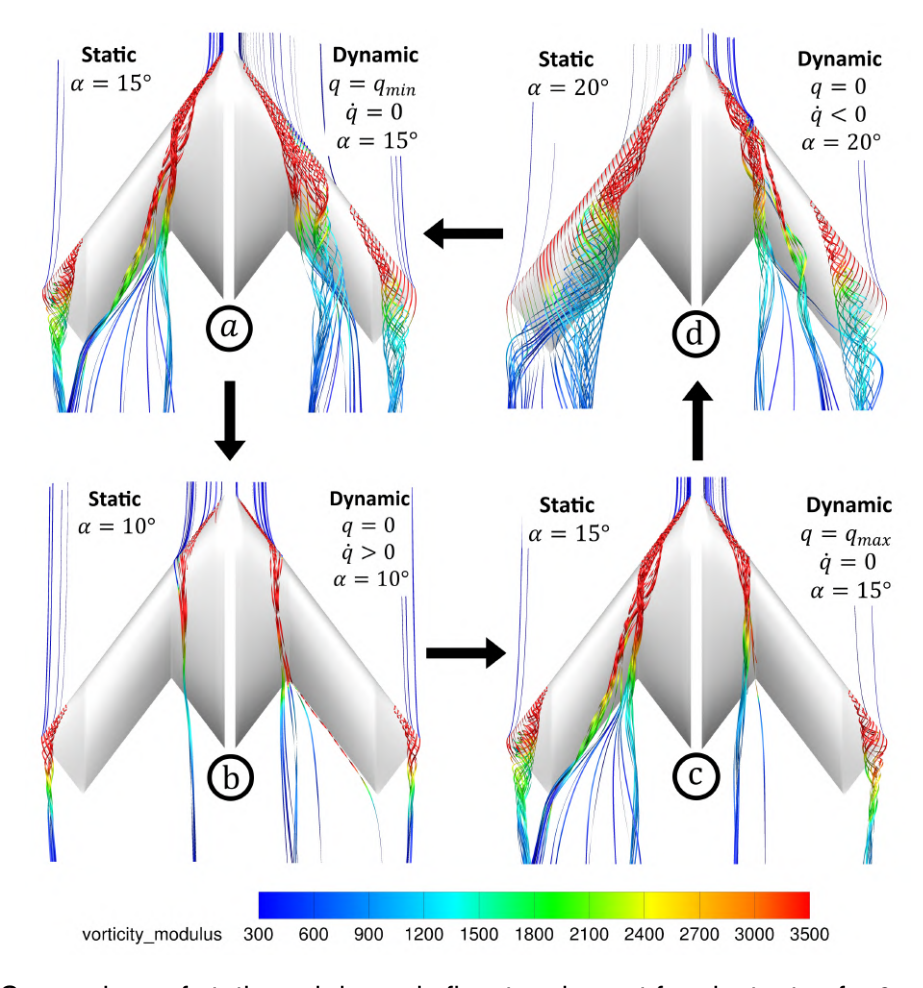
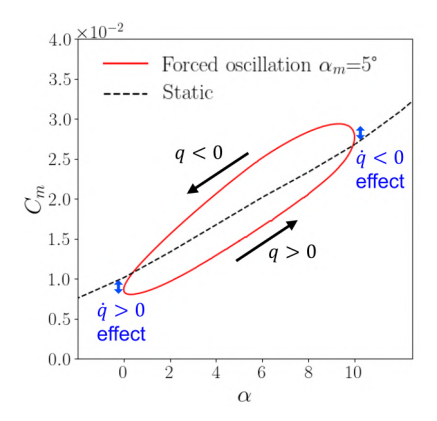


Figure 11 – Comparison of static and dynamic flow topology at four instants of a 3 H_Z pitch forced oscillation period ($\omega^* = 0.11497$) of 5° amplitude centered on a mean angle of $\alpha_m = 15$ °

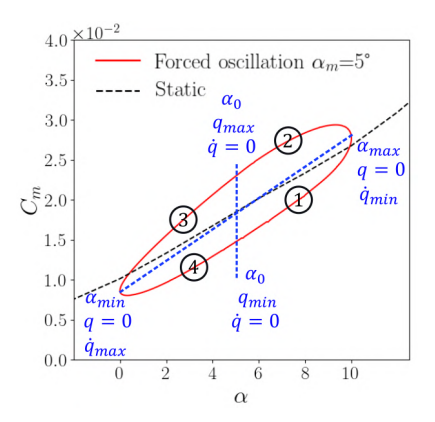
5.3 Multi-Identification Model

5.3.1 Identification Process

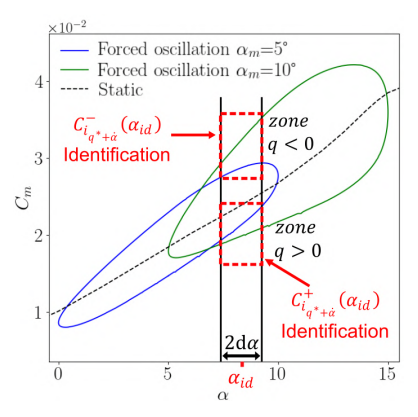
A new model based on a multi-stage identification process is presented in this section, in order to improve the modelling produced by the QS model. To this end, three characteristics of the vortex flow observed in the previous section are taken into account in this ROM. Firstly, vortex dynamics are fast over an oscillation period. This implies that the stability derivatives of the QS model must be considered as variable during an oscillation period. Secondly, the identification of the stability derivatives must be different for the increase (q > 0) or the decrease (q < 0) of the AOA (figure 12a). Finally,



(a) Representation of dynamic effects related to the effects of q and *a*



(b) Presentation of model identification zones for an oscillation loop



(c) Representation of the identification zones of $C^+_{i_{q^*+\alpha^*}}$ and $C^-_{i_{q^*+\dot{lpha}^*}}$ at $lpha_{id}$ depending on the sign of q an the value of $d\alpha$

Figure 12 – Identification process

the unsteady effects due to variation in the rotation rates (\dot{q} effects) have to be taken into account (figure 12a). These effects also have to be identified differently according to the increase ($\dot{q} > 0$) or the decrease $(\dot{q} < 0)$ of the rotation rate. These observations lead us to divide a forced oscillation period into four zones delimited by four characteristic points of the oscillation corresponding to the following flight parameters: $(\alpha = \alpha_0, q = q_{min}, \dot{q} = 0)$, $(\alpha = \alpha_{min}, q = 0, \dot{q} = \dot{q}_{max})$, $(\alpha = \alpha_0, q = q_{max})$ $\dot{q}=0$) and $(\alpha=\alpha_{max},\ q=0,\ \dot{q}=\dot{q}_{min})$ (figure 12b). The multi-identification model, introduced in this section, has four different formulations depending on the zone in which the model is applied. The formulation of the model according to the different zones is written as:

- $$\begin{split} \bullet \text{ zone 1} & \to q > 0 \text{ and } \dot{q} < 0 : C_i(t) = C_{i_0}(\alpha(t)) + C^+_{i_{q^*}+\alpha^*}(\alpha(t))q^*(t) + C^-_{i_{q^*}}(\alpha(t))\dot{q}^*(t) \\ \bullet \text{ zone 2} & \to q < 0 \text{ and } \dot{q} < 0 : C_i(t) = C_{i_0}(\alpha(t)) + C^-_{i_{q^*}+\alpha^*}(\alpha(t))q^*(t) + C^-_{i_{q^*}}(\alpha(t))\dot{q}^*(t) \\ \bullet \text{ zone 3} & \to q < 0 \text{ and } \dot{q} > 0 : C_i(t) = C_{i_0}(\alpha(t)) + C^-_{i_{q^*}+\alpha^*}(\alpha(t))q^*(t) + C^+_{i_{q^*}}(\alpha(t))\dot{q}^*(t) \\ \bullet \text{ zone 4} & \to q > 0 \text{ and } \dot{q} > 0 : C_i(t) = C_{i_0}(\alpha(t)) + C^+_{i_{q^*}+\alpha^*}(\alpha(t))q^*(t) + C^+_{i_{q^*}}(\alpha(t))\dot{q}^*(t) \end{split}$$

Where $C_{i_0}(\alpha(t))$ represents the static coefficient taken at $\alpha(t)$. The coefficients $C^+_{i_{q^*+\alpha^*}}$ and $C^-_{i_{q^*+\alpha^*}}$ are the out-phase derivatives evaluated respectively when the AOA increases (q > 0) and decreases (q < 0). Finally, the coefficients $C_{i_{a^*}}^+$ and $C_{i_{a^*}}^-$ correspond to the derivatives associated with the \dot{q} effect for a positive $(\dot{q} > 0)$ and negative $(\dot{q} < 0)$ variation in the rotation rate. Thus, these stability derivatives will vary as a function of the AOA but also according to the sign of the rotation rate q or its derivative \dot{q} . The first identification step of this model is to evaluate the coefficients $C_{i_{a^*}}^+$ and $C_{i_{a^*}}^-$. These terms are identified at the extremities of the oscillation loops (figure 12a) at the minimum ($\alpha=\alpha_{min}$) and maximum ($\alpha=lpha_{max}$) AOA (figure 12b) for which ($q=0,\ \dot{q}_{max}=\dot{q}(lpha_{min})$) and ($q=0,\ \dot{q}_{min}=\dot{q}(lpha_{max})$). They are computed, at these two points of the oscillation, as the difference between the aerodynamic coefficient obtained during a forced oscillation C_i^{osc} and the static coefficient C_{io} :

$$C_{i_{\dot{q}^*}}^{+} = \frac{C_i^{osc}(\alpha_{min}) - C_{i_0}(\alpha_{min})}{\dot{q}^*(\alpha_{min})} \qquad C_{i_{\dot{q}^*}}^{-} = \frac{C_i^{osc}(\alpha_{max}) - C_{i_0}(\alpha_{max})}{\dot{q}^*(\alpha_{max})}$$
(9)

Identification is carried out on all simulated forced oscillations having a different mean angle but with identical amplitude and frequency. The values of both coefficients depend on the AOA and are assumed to vary linearly between the identification points (figure 13a, b and c). The difference between these coefficients shows the importance of taking into account the sign of the variation of the rotation rate \dot{q} . The second identification step consists in identifying the terms $C^+_{i_q^*+\alpha^*}$ and $C^-_{i_q^*+\alpha^*}$. In contrast to the classical linear QS model, these stability derivatives are assumed to be variable over an oscillation loop. This allows, in particular, to take into account the rapid evolution of the vortex

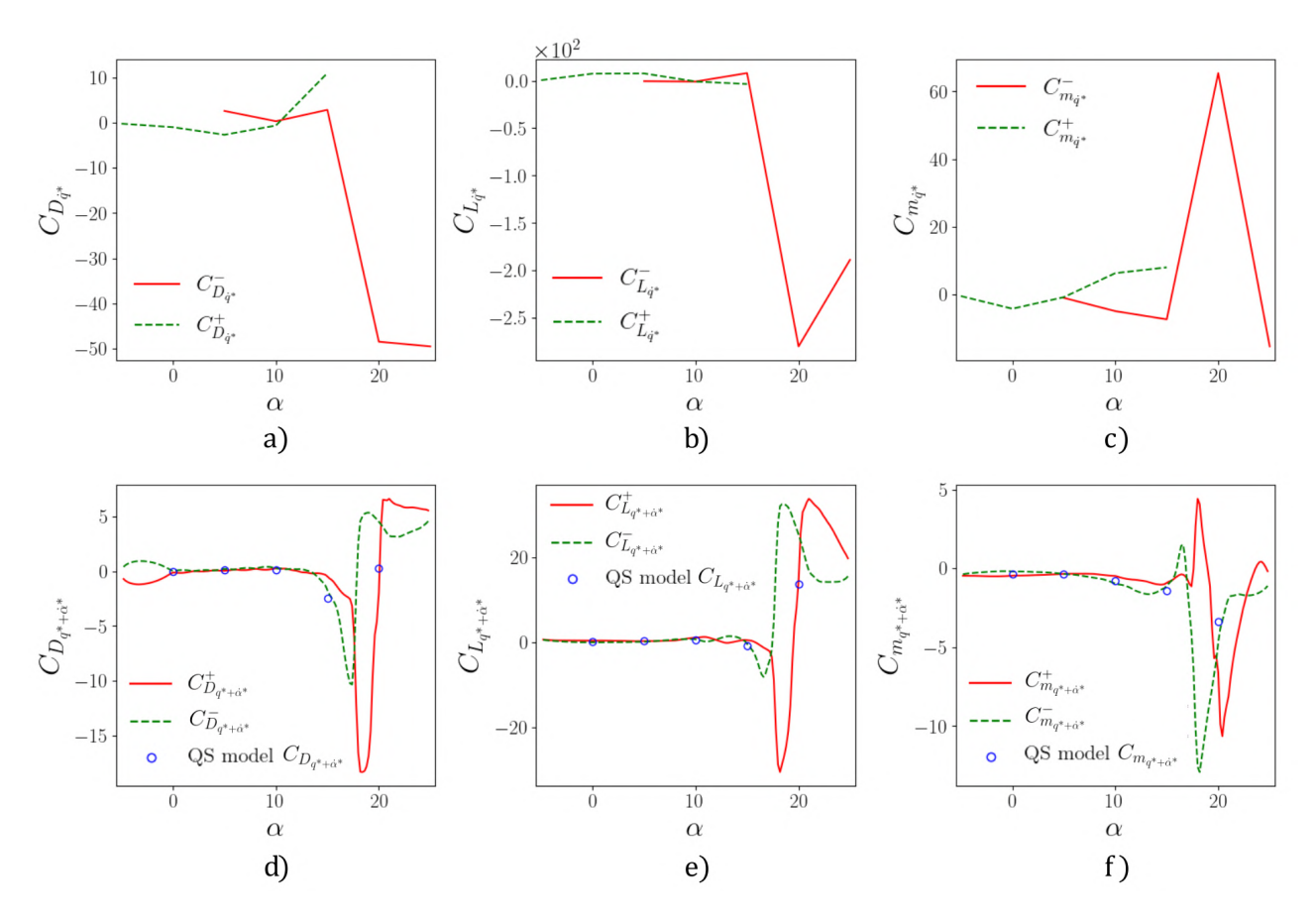


Figure 13 – Parameters of the multi-identification model as a function of the AOA determined from 1 Hz pitch forced oscillations ($\omega^* = 0.03832$) of 5° amplitude

dynamic compared with an oscillation period. The database generated from the CFD simulations is composed of the results of different forced oscillations which overlap over different AOA ranges (figure 6). Thus, by considering each forced oscillation separately, discontinuities in $C^+_{i_q^*+\dot{\alpha}^*}$ and $C^-_{i_q^*+\dot{\alpha}^*}$ as a function of AOA can be observed, as with the NASA method [12]. In order to ensure the continuity of these coefficients with the AOA, the identification must be carried out taking into account the different loops that are superimposed for a given angle of attack. Thus, the stability derivatives $C^+_{i_{q^*+\dot{\alpha}^*}}$ and $C^-_{i_{q^*+\dot{\alpha}^*}}$ are identified for a certain AOA noted α_{id} by performing a least squares method on all the points in the database belonging to an interval $[\alpha_{id}-d\alpha;\alpha_{id}+d\alpha]$ for which the rotation rate is respectively positive (q<0) and negative (q<0) (figure 12c). Knowing that the static coefficients C_{i_0} and the stability derivatives $C^+_{i_{q^*}}$ and $C^-_{i_{q^*}}$ are already known, the minimization of the model error with respect to the CFD coefficients of the forced oscillations C^{osc}_i is written as follows:

$$C_{i_{q^*+\alpha^*}}^{+}(\alpha_{id}) = \underset{x}{\operatorname{argmin}} \sum_{j=0}^{n_l} \sum_{k=0}^{n_p^j} W_1 \left(\Delta C_i^j(t_k) - x q_j^*(t_k) \right)^2$$

$$C_{i_{q^*+\alpha^*}}^{-}(\alpha_{id}) = \underset{x}{\operatorname{argmin}} \sum_{j=0}^{n_l} \sum_{k=0}^{n_p^j} W_2 \left(\Delta C_i^j(t_k) - x q_j^*(t_k) \right)^2$$
(10)

With

$$\Delta C_{i}^{j}(t_{k}) = \begin{cases} C_{i}^{osc,j}(t_{k}) - C_{i_{0}}(\alpha_{j}(t_{k})) - C_{i_{q^{*}}}^{+}(\alpha_{j}(t_{k}))\dot{q}_{j}^{*}(t_{k}) & \text{if } \dot{q}_{j}^{*}(t_{k}) > 0 \\ C_{i}^{osc,j}(t_{k}) - C_{i_{0}}(\alpha_{j}(t_{k})) - C_{i_{q^{*}}}^{-}(\alpha_{j}(t_{k}))\dot{q}_{j}^{*}(t_{k}) & \text{else} \end{cases}$$

$$(11)$$

And

$$W_1 = \begin{cases} 1 & \text{if } \alpha_j(t_k) \in [\alpha_{id} - d\alpha; \alpha_{id} + d\alpha] \text{ and } q_j^*(t_k) > 0 \\ 0 & \text{else} \end{cases}$$

$$W_2 = \begin{cases} 1 & \text{if } \alpha_j(t_k) \in [\alpha_{id} - d\alpha; \alpha_{id} + d\alpha] \text{ and } q_j^*(t_k) < 0 \\ 0 & \text{else} \end{cases}$$

$$(12)$$

Where n_l is the number of different forced oscillations in the data base (5 in the context of our study) and n_p^j the number of time step in a period of the jth forced oscillation. The parameters $\alpha_j(t_k)$ and $q_j^*(t_k)$ represents the AOA and the rotation rate at time $t_k = k\Delta t$ related to the jth forced oscillation of the database. This identification process is carried out every $d\alpha$. The choice of the value of $d\alpha$ and the thickness of the identification range is discussed in the next section. The results obtained for $d\alpha = 0.2$ are shown in figure 13d, e and f. Both coefficients, $C_{i_{q^*+\alpha^*}}^+$ and $C_{i_{q^*+\alpha^*}}^-$, are almost identical as long as there is no vortex on the upper surface of the wing ($\alpha < 10^\circ$). The differences between them are becoming increasingly pronounced as vortex dynamics develops. This justifies the identification distinction as a function of the sign of the rotation rate q. The values of the stability derivatives of the linear QS model overlap at least one of the multi-identification coefficient (13d, e and f). Thus, identification problems of the linear QS model stem from the fact that there are not enough points identified to capture the strong non-linearities and there is no difference according to the sign of the rotation rate q.

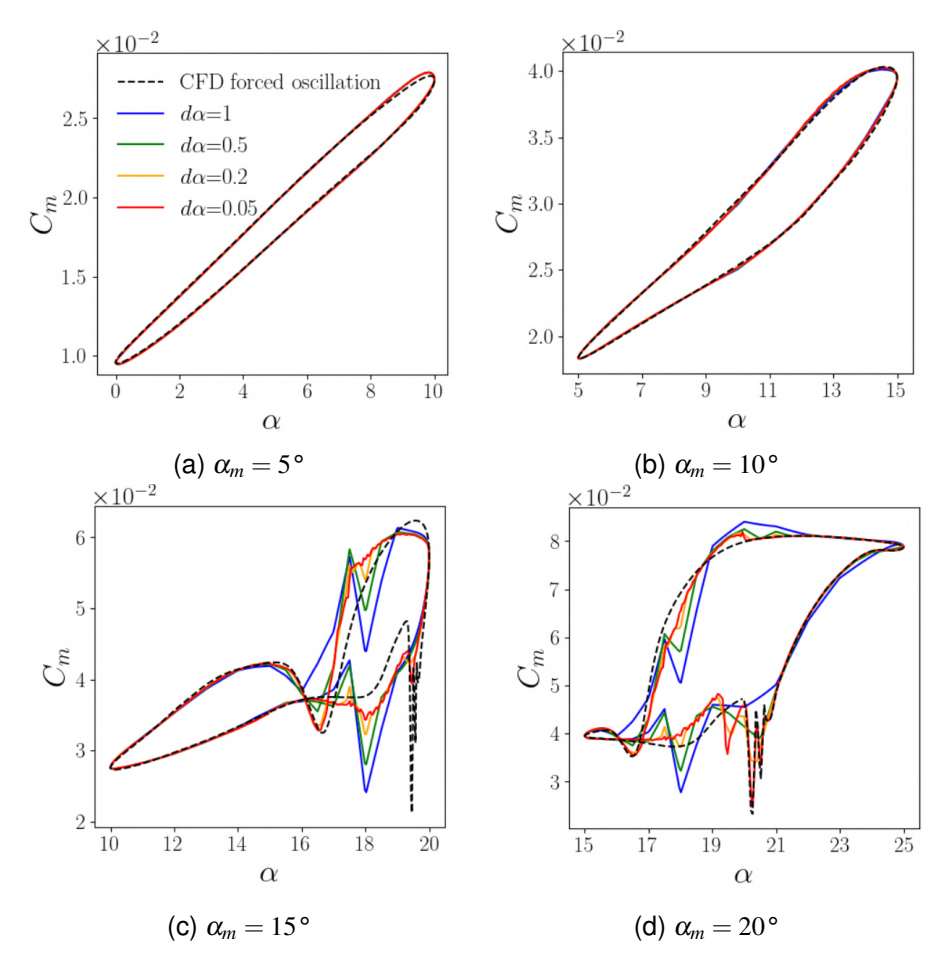


Figure 14 – Comparison between the changes in the pitch coefficient C_m obtained by CFD calculation and by the multi-identification model for different steps of identification $d\alpha$ during 1 H_Z pitch forced oscillation period ($\omega^* = 0.03832$) of 5° amplitude centered in different mean angles α_m

5.3.2 Sensitivity of the Multi-Identification Model to the Parameters $d\alpha$

A parametric study of the influence of the thickness of the identification zone $[\alpha_{id} - d\alpha; \alpha_{id} + d\alpha]$ is carried out on the changes in the pitch coefficient C_m during 1 Hz pitch forced oscillations ($\omega^* = 0.03832$) of 5° amplitude centered in four different mean angles α_m (figure 14). To this end, the stability derivatives $C_{i_q^*+\alpha^*}^+$ and $C_{i_q^*+\alpha^*}^-$ are identified for different values of $d\alpha$. Then, the multi-identification model is applied and compared with CFD data. It appears that when the vortex flow is not established ($\alpha < 10$ °) or is only slightly developed (from $\alpha = 10$ ° to 14°), the choice of the value of $d\alpha$ has little influence (figure 14a and 14b). On the other hand, when the motion enters in the non-linear domain, where the behaviour of the aerodynamic coefficients is dominated by the vortex flow ($\alpha > 15$ °), significant differences in the restitution of the pitch coefficient are observed as a function of the $d\alpha$ value (figure 14c and 14d). If the parameter $d\alpha$ is chosen too large, the non-linear behaviour fails to be correctly modeled. The coefficients are considered constant over a range of AOA that is too wide, which brings us back to the problem of the initial identification of the linear QS model. The smaller the step size, the more accurate the modeling becomes, but the parameters becomes noisy. To limit noise in parameter values, a step size of $d\alpha = 0.2$ ° is chosen for the study.

5.4 Application and Comparison of the ROMs

The multi-identification model is compared with the linear QS model and with the non-linear indicial method for which the results are taken from Isnard et al. [5]. The performance of these different ROMs is compared in terms of their ability to reproduce the changes in the aerodynamic coefficients during an imposed trajectory. To do this, a study of the overall and instantaneous accuracy of the ROMs is carried out on a $1\,H_Z$ pitch forced oscillation period ($\omega^* = 0.03832$) of $5\,^{\circ}$ amplitude centered on a mean angle of $\alpha_m = 15\,^{\circ}$ (figure 15). Qualitatively, it is clear that the multi-identification model reproduces more accurately the non-linear behaviour and the trends of the pitch coefficient C_m than the other two models (figure 15a). This leads to a higher coefficient of determination ($R^2 = 0.9493$) than

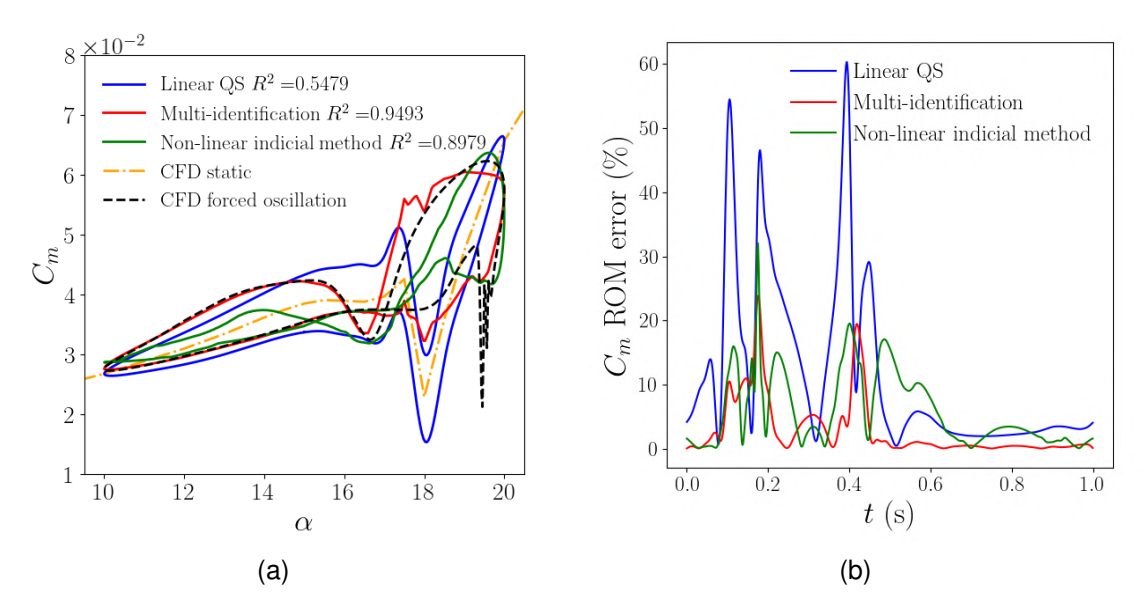


Figure 15 – Comparison between the chnages in the pitch coefficient C_m obtained by CFD calculation and by different ROMs a), and the associated instantaneous error b) during a 1 Hz pitch forced oscillation period ($\omega^* = 0.03832$) of 5° amplitude centered on a mean angle of $\alpha_m = 15$ °

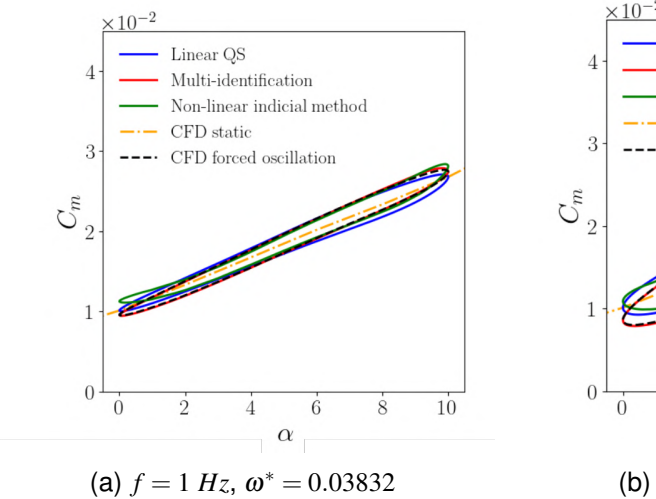
that of the indicial method ($R^2=0.8979$) and the linear QS model ($R^2=0.5479$). In addition, the instantaneous error of the multi-identification model is reduced in both the linear and non-linear phases of the movement compared with the linear QS model (figure 15b). For AOA values above $\alpha=15^{\circ}$ (corresponding to t between 0 and 0.5 s), the instantaneous error is lower than for the other two models and is almost always kept below 10% with a peak at 20% (compared with 60% for the linear QS model and 30% for the indicial method). Similarly, for AOA values below $\alpha=15^{\circ}$ (corresponding to t between 0.5 and 1 s), the instantaneous error is almost zero. This shows that the multi-identification

model is more efficient at modelling the changes in the pitch coefficients in the non-linear domain as well as in the linear domain. The aim of this section is to show that the multi-identification model outperforms the linear QS model and the indicial method in reproducing pitch forced oscillation loops of 5° amplitude for different frequencies, different mean angles and for all the longitudinal aerodynamic coefficients. To do this, the different ROMs are applied to reproduce the changes in the drag, lift and pitch coefficients during pitch forced oscillations. The coefficients of determination R^2 obtained, are presented in Table 2.

Table 2 – Coefficient of determination R^2 of the different ROMs studied for forced oscillations of 5° amplitude with different frequencies and mean angles.

		C_D			C_L			C_m		
α_m	f	R_{QS}^2	R_{Ind}^2	$R^2_{Multi-id}$	R_{QS}^2	R_{Ind}^2	$R^2_{Multi-id}$	R_{QS}^2	R_{Ind}^2	$R^2_{Multi-id}$
5	1	0.9996	0.5908	0.9999	0.9999	0.9994	0.9999	0.9975	0.9862	0.9997
10	1	0.9907	0.8930	0.9997	0.9997	0.9991	0.9999	0.9883	0.9815	0.9996
15	1	0.9646	0.9182	0.9974	0.9692	0.9629	0.9977	0.5479	0.8979	0.9493
20	1	0.9748	0.8391	0.9994	0.8603	0.9221	0.9971	0.7473	-0.1218	0.9889
5	2	0.9990	0.5965	0.9998	0.9999	0.9993	0.9999	0.9864	0.9823	0.9980
10	2	0.9442	0.8788	0.9930	0.9976	0.9992	0.9995	0.9675	0.9513	0.9734
15	2	0.9011	0.7071	0.9789	0.9495	0.9536	0.9817	-0.6559	0.4335	0.6376
20	2	0.9463	0.8615	0.9957	0.7389	0.8939	0.9830	0.6891	-0.0003	0.9474
5	3	0.9987	0.6043	0.9996	0.9997	0.9991	0.9999	0.9772	0.9750	0.9964
10	3	0.9674	0.8544	0.9923	0.9988	0.9992	0.9999	0.9587	0.9036	0.9892
15	3	0.6770	0.3010	0.9962	0.9545	0.9858	0.9918	-0.525	0.1575	0.7338
20	3	0.9318	0.8788	0.9977	0.6739	0.8437	0.9902	0.6606	0.006	0.9417

For all the configurations studied, the overall accuracy of the multi-identification model is better than the other two models for all the longitudinal coefficients. As with the other ROMs, a deterioration in the performance of the model is observed as the AOA and the frequency increase. This loss of performance with increasing frequency is relatively small for pitch forced oscillations centred on $\alpha_m = 5^{\circ}$ and $\alpha_m = 10^{\circ}$. However, The multi-identification model fits the CFD data more accurately than the linear QS model or the indicial method for the pitch oscillations centred on $\alpha_m = 5^{\circ}$ (figure 16). Nonetheless, increasing deviations between CFD data and the multi-identification model are observed around $\alpha = 10^{\circ}$ as the frequency increases (figure 16), which can explains the decrease in the value of R^2 .



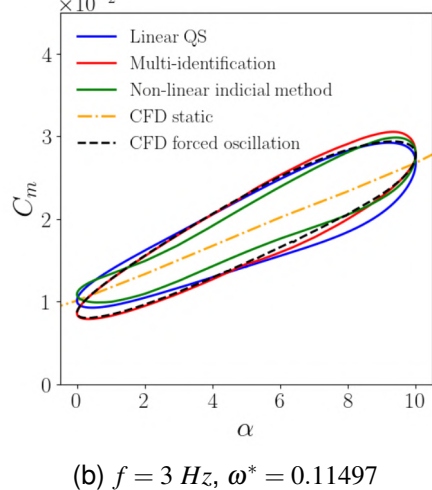


Figure 16 – Comparison between the changes in the pitch coefficient C_m obtained by CFD calculation and by different ROMs during a pitch forced oscillation period of 5° amplitude centered on a mean angle of $\alpha_m = 5^{\circ}$ for different frequencies

In this linear domain, for pitch oscillations centred on $\alpha_m = 5\,^{\circ}$ and $\alpha_m = 10\,^{\circ}$, the coefficient of determination of the multi-identification model for C_m remains greater than 0.97 at any frequency. When the non-linear domain is reached, for pitch oscillations centred on $\alpha_m = 15\,^{\circ}$ and $\alpha_m = 20\,^{\circ}$, the accuracy of the model decreases (remaining above 0.6376) but does not drop as much as the linear QS model or the indicial method, for which the coefficient of determination R^2 can be negative. Qualitatively, the multi-identification model is no longer able to match the CFD data, but the C_m trends and the non-linearities are still reproduced correctly for all frequencies. In contrast, the linear QS model is unable to reproduce these non-linearities and the indicial method does not always reproduce them correctly depending on the frequency or the AOA (figure 17). This explains why the coefficient of determination of the multi-identification model is much higher in the non-linear domain for C_m .

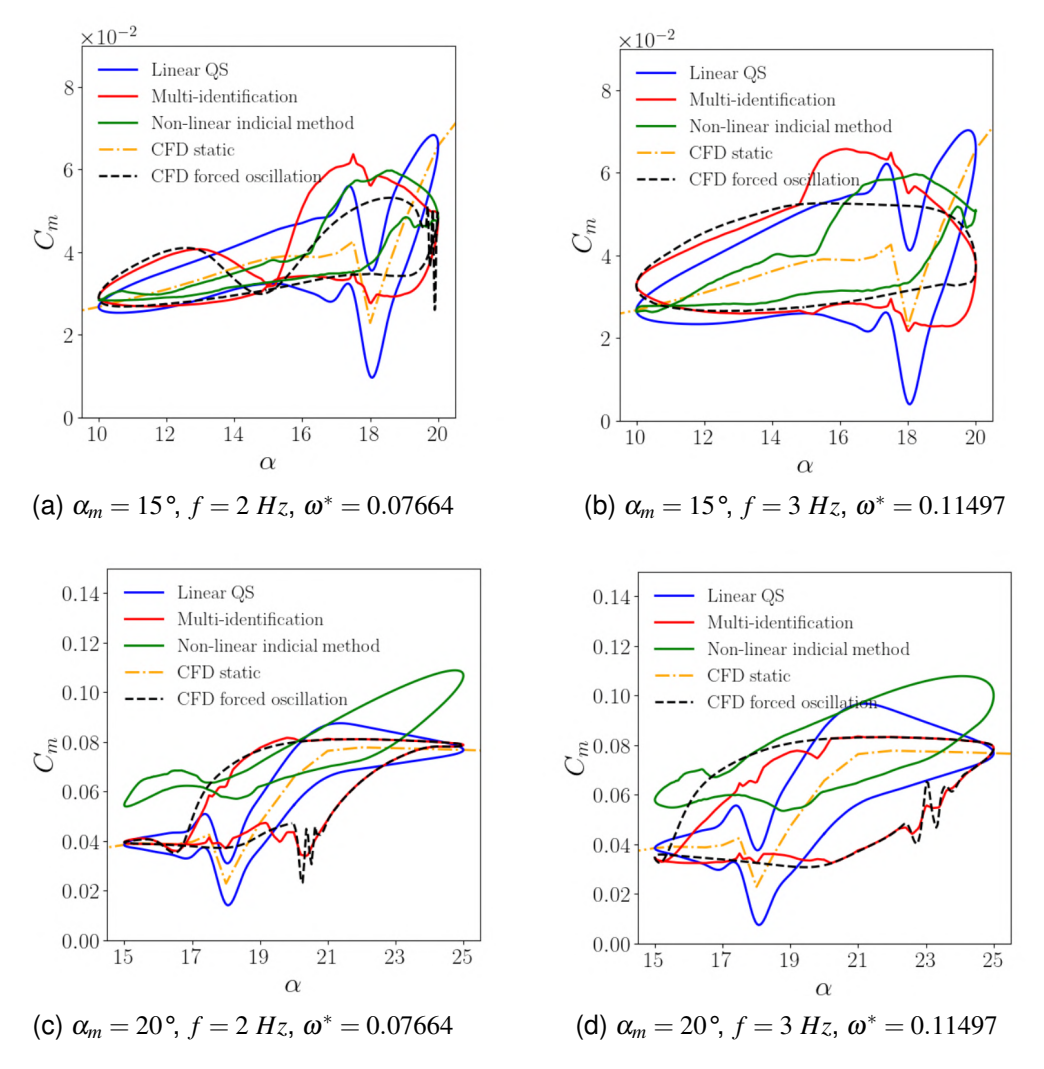


Figure 17 – Comparison between the changes in the pitch coefficient C_m obtained by CFD calculation and by different ROMs during a pitch forced oscillation period of 5° amplitude centered on different mean angles for different frequencies

Finally, the model is also applied to the lift and drag coefficients. The coefficient of determination R^2 of the multi-identification model is greater than 0.9798 for the C_D and 0.9817 for the C_L for all AOAs and all oscillation frequencies. Thus, its overall accuracy remains well above that of the linear QS model and the indicial method. Qualitatively, as with the modelling of the C_m , the multi-identification model is capable of modelling the non-linearities present in the drag C_D (figure 18) and lift C_L (figure 19) coefficients, unlike the linear QS model and the indicial method which are unable to do so.

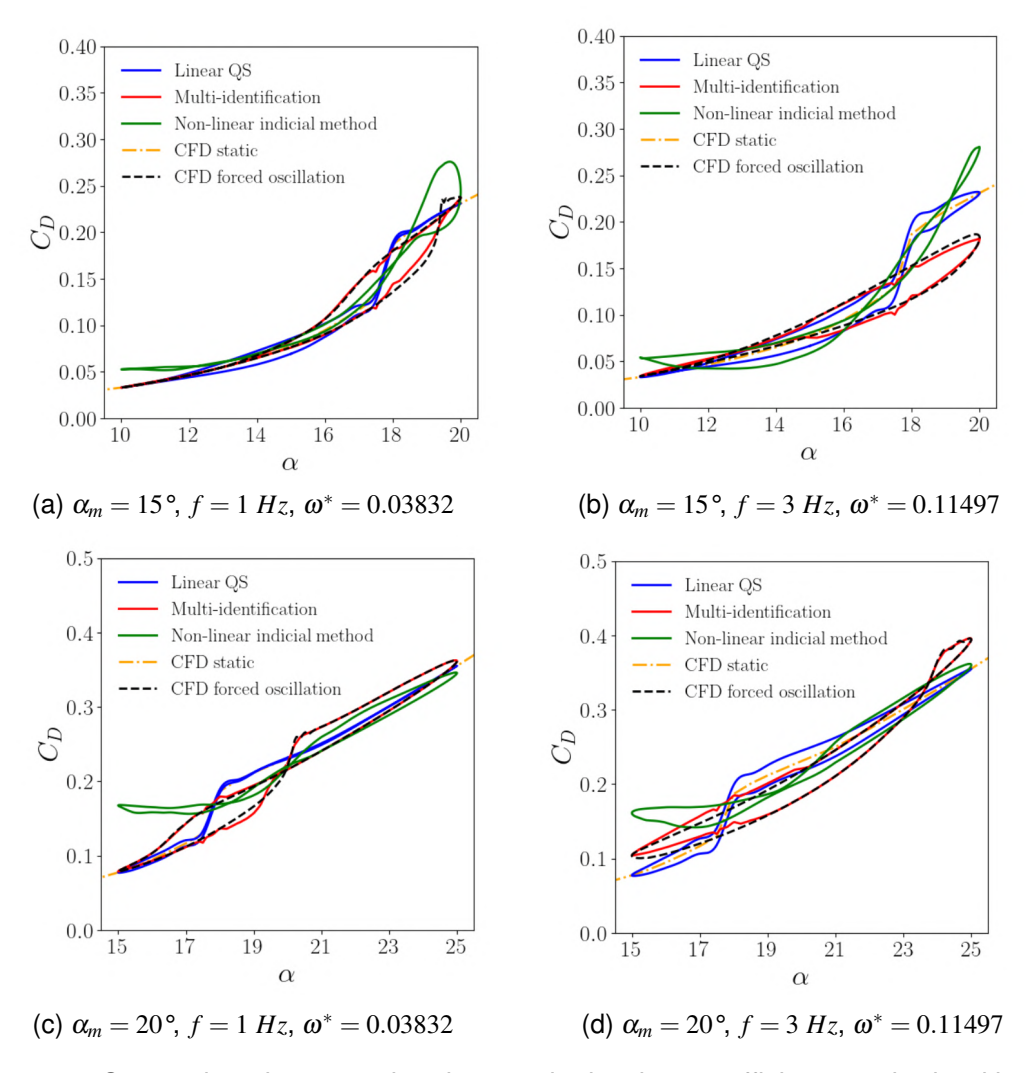


Figure 18 – Comparison between the changes in the drag coefficient C_D obtained by CFD calculation and by different ROMs during a pitch forced oscillation period of 5° amplitude centered on different mean angles for different frequencies

6. Conclusion and Prospects

This paper investigates the use of the linear QS model to predict the unsteady and non-linear longitudinal aerodynamics of a UCAV configuration thanks to CFD simulations using grid motions. In a first step of the analysis, the pros and the cons of the classical linear QS model are discussed. Then, this paper proposes an improvement of this ROM.

The study of the linear QS model shows that it is accurate for modelling aerodynamic coefficients during a trajectory in the linear domain, at low incidence. However, it is unable to reproduce the unsteady effects and non-linearities that appear at high angles of attack. These modelling discrepancies are caused by an incorrect assumption made during the identification process. Indeed, the study of the flow topology during pitch forced oscillations has shown that the vortex dynamics change rapidly compared with a oscillation period. This proves that assuming that the stability derivatives are constant over this kind of trajectories is not correct particularly at high AOA where the aircraft's behaviour is directly related to the vortex dynamics. Moreover, different impacts of the motion on the flow topology are identified as a function of the increasing or decreasing angle of attack and rotation rate.

A multi-identification model is developed to take into account the informations about the flow dynamics related to the motion into the identification process of the stability derivatives. This model requires the same amount of data as the linear QS model in order to be implemented. In adddition, it proves to be much more accurate than the linear QS model and the indicial method for modelling aerodynamic

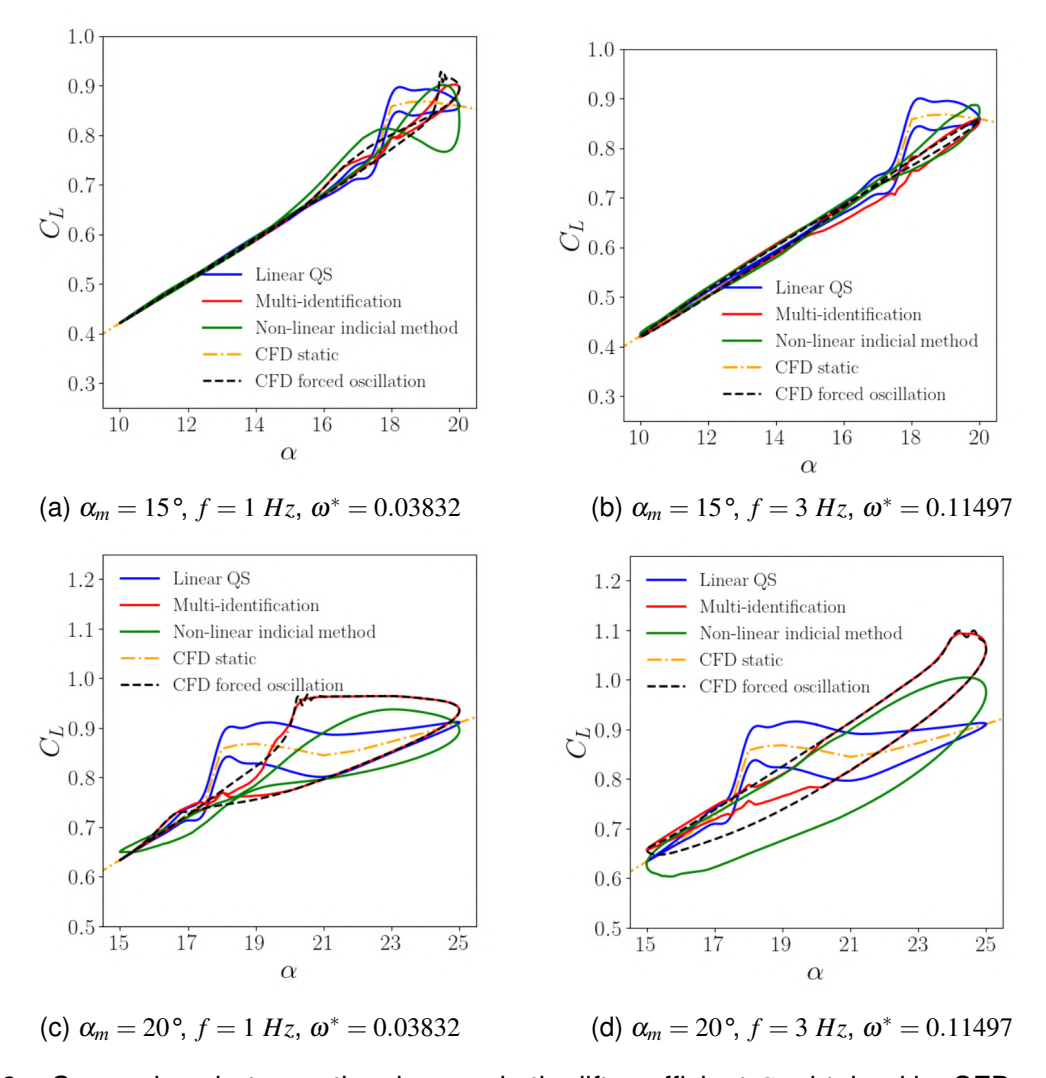


Figure 19 – Comparison between the changes in the lift coefficient C_L obtained by CFD calculation and by different ROMs during a pitch forced oscillation period of 5° amplitude centered on different mean angles for different frequencies

coefficients in the linear and non-linear flight domains.

Future work will aim to improve the multi-identification model. One possibility would be to incorporate a new physical parameter corresponding to a delay in the vortex development during a motion. Another way for improving this new model would be to carry out plunging simulations to decouple the parameters q and $\dot{\alpha}$ obtained with the study of forced oscillations in pitch. Finally, it will be interesting to see whether the multi-identification model performs as well on other geometries and other types of trajectory.

7. Acknowlegment

The authors gratefully acknowledge the financial support given by ONERA and the region Hauts-de-France. The authors appreciate the support provided by the elsA software technical assistance. SAC-CON (Stability and Control Configuration) geometry and wind-tunnel data were provided by NATO RTO Task Group AVT-161 on Assessment of Stability and Control Prediction Methods for NATO Air and Sea Vehicles.

8. Contact Author Email Address

mailto: baptiste.isnard@onera.fr mailto: dominique.farcy@onera.fr

9. Copyright Statement

The authors confirm that they, and/or their company or organization, hold copyright on all of the original material included in this paper. The authors also confirm that they have obtained permission, from the copyright holder of any third party material included in this paper, to publish it as part of their paper. The authors confirm that they give permission, or have obtained permission from the copyright holder of this paper, for the publication and distribution of this paper as part of the ICAS proceedings or as individual off-prints from the proceedings.

References

- [1] Vallespin D. Development of a process and toolset to study UCAV flight mechanics using computational fluid dynamics. *Thesis, University of Liverpool, UK*, 2011.
- [2] Ghoreyshi M, Jirásek A, and Cummings R. M. Reduced order unsteady aerodynamic modeling for stability and control analysis using computational fluid dynamics. *Progress in Aerospace Sciences*, Vol. 71, pp 167-217, 2014.
- [3] Widhalm M, Stradtner M, Schütte A, Ghoreyshi M, Jirasek A, and Seidel J. Comparison of Reduced Order Models for Evaluating Stability Derivatives for the DLR-F22 ONERA model. *AIAA AVIATION Forum*, 2023.
- [4] Rohlf D, Schmidt S, and Irving J. SACCON Stability and Control Analyses Applying System Identification Techniques. *28th AIAA Applied Aerodynamics Conference*, 2010.
- [5] Isnard B, Tanguy G, Farcy D, Dugeai A, Garnier E, and Foucaut J.M. Accuracy and Computational Cost Comparison of Numerical Reduced Order Models of a Generic UCAV Configuration (currently being submitted). *AIAA Journal*, 2024.
- [6] Hiller B. R. *An Unsteady Aerodynamics Reduced-Order Modeling Method For Maneuvring, Flexible Flight Vehicles.* Thesis, Georgia Institute of Technology, USA, 2019.
- [7] Le Roy J.F, Morgand S, and Farcy D. Static and Dynamic Derivatives on generic UCAV without and with leading edge control. *32nd AIAA Applied Aerodynamics Conference*, 2014.
- [8] Allen J. D, Ghoreyshi M, Jirasek A, and Satchell M. Aerodynamic Loads Identification and Modeling of UCAV Configurations with Control Surfaces Using Prescribed CFD Maneuvers. *2018 Applied Aerodynamics Conference*, 2018.
- [9] Bommanahal M. V. *Nonlinear Modeling and Identification of Unsteady Aerodynamics at Stall.* Thesis, Faculty of Technology, De Montfort University, UK, 2015.
- [10] Zhou C, Zhu J, and Lei H. Aircraft Longitudinal Unsteady Aerodynamic Modeling Using Indicial Function. *IEEE Chinese Guidance, Navigation and Control Conference*, 2016.
- [11] Da Ronch A, Vallespin D, Ghoreyshi M, and Badcock K. J. Evaluation of Dynamic Derivatives Using Computational Fluid Dynamics. *AlAA Journal*, Vol. 50, No. 2, pp 470-484, 2012.
- [12] Vicroy D. D. A Guide to Forced Oscillation Data Processing and Analysis. *NASA-TP-20210023569*, 2023.
- [13] Kirschstein S and Alles W. Identification of dynamic derivatives with a controlled wind tunnel model of the spaceplane-configuration PHOENIX. *Aerospace Science and Technology*, Vol. 8, No. 6, pp 509-518, 2004
- [14] Wang Z, Lan C, and Brandon J. Unsteady aerodynamic effects on the flight characteristics of an F-16XL configuration. *Atmospheric Flight Mechanics Conference*, 2000.
- [15] Planckaert L. Model of Unsteady Aerodynamic Coefficients of a Delta Wing aircraft at high angles of attack. *Vortex Flow and High Angle of Attack Aerodynamics*, 2001.
- [16] Cummings R and Schütte A. An Integrated Computational/Experimental Approach to UCAV Stability & Stability
- [17] Morgand S. Caractérisation et contrôle de l'écoulement autour d'un UCAV générique. *Thesis, Université Pierre et Marie Curie Paris VI, Fr*, 2013.
- [18] Cambier L and Veuillot J.P. Status of the elsA Software for Flow Simulation and Multi-Disciplinary Applications. *46th AIAA Aerospace Sciences Meeting and Exhibit*, 2008.
- [19] Cambier L, Heib S, and Plot S. The onera elsa cfd software: input from researchand feedback from industry. *Mechanics & Industry*, Vol. 14, No. 3, pp 159–174, 2013.
- [20] Roache P. J. Perspective: A Method for Uniform Reporting of Grid Refinement Studies. *Journal of Fluids Engineering*, Vol. 116, No. 3, pp 405-413, 1994.
- [21] Spalart P and Allmaras S. A one-equation turbulence model for aerodynamic flows. *30th Aerospace Sciences Meeting and Exhibit*, 1992.

- [22] Jameson A, Schmidt W, and Turkel E. Numerical solution of the Euler equations by finite volume methods using Runge Kutta time stepping schemes. *14th Fluid and Plasma Dynamics Conference*, 1981.
- [23] Harten A. High resolution schemes for hyperbolic conservation laws. *Journal of Computational Physics*, Vol. 49, No. 3, pp 357-393, 1983.
- [24] Choi Y. H and Merkle C. L. The Application of Preconditioning in Viscous Flows. *Journal of Computational Physics*, Vol. 105, No. 2, pp 207-223, 1993.
- [25] Weiss J. M and Smith W. A. Preconditioning applied to variable and constant density flows. *AIAA Journal*, Vol. 33, No. 11, pp 2050-2057, 1995.
- [26] Gear C. W. *Numerical Initial Value Problems in Ordinary Differential Equations*. Prentice-Hall, Upper Saddle River, USA, 1971.
- [27] Loeser T, Vicroy D, and Schütte A. SACCON Static Wind Tunnel Tests at DNW-NWB and 14 x22 NASA LaRC. 28th AIAA Applied Aerodynamics Conference, 2010.
- [28] Cummings R. M and Schütte A. Integrated Computational/Experimental Approach to Unmanned Combat Air Vehicle Stability and Control Estimation. *Journal of Aircraft*, Vol. 49, No. 6, pp 1542-1557, 2012.
- [29] Farcy D. Essais dynamiques et identification sur maquette SACCON Participation au groupe RTO/AVT161, ONERA Internal Report, RT1/19066 DCSD, 2011.
- [30] Farcy D. SACCON-ONERA-SV4-rotarybalance-tests, ONERA Internal Report, DCSD-2011-003-NOT-002-1.0, 2012.
- [31] Ghoreyshi M and Cummings R. M. Unsteady aerodynamics modeling for aircraft maneuvers: A new approach using time-dependent surrogate modeling. *Aerospace Science and Technology*, Vol. 39, pp 222-242, 2014.
- [32] Schütte A, Hummel D, and Hitzel S M. Numerical and experimental analyses of the vortical flow around the SACCON configuration. *28th AIAA Applied Aerodynamics Conference*, 2010.
- [33] Gray J. S, Hwang J. T, Martins J. R. R. A, Moore K. T, and Naylor B. A. OpenMDAO: An open-source framework for multidisciplinary design, analysis, and optimization. *Structural and Multidisciplinary Opti*mization, Vol. 59, No. 4, pp 1075-1104, 2019.
- [34] Sacks J, Welch W. J, Mitchell T. J, and Wynn H. P. Design and Analysis of Computer Experiments. Statistical Science, Vol. 4, No. 4, pp 409-423, 1989.
- [35] Byrd R. H, Lu P, Nocedal J, and Zhu C. A Limited Memory Algorithm for Bound Constrained Optimization. *SIAM Journal on Scientific Computing*, Vol. 16, No. 5, pp 1190-1208, 1995.